Max von Pettenkofer and his Life

Honorary Member Tatsuaki TANAKA (Ochanomizu University)

The author studied architecture at university and first encountered Pettenkofer's ventilation theory in Professor Koichiro Kimura's "Architectural Health Engineering" course. This sparked a lasting interest in Pettenkofer. In July 2024, the author visited Munich to research him, exploring the Pettenkofer Institute at Munich University and the Fraunhofer Institute for Building Physics. They also visited Pettenkofer's statue, grave, the water source he introduced to Munich, and a street named after him. Additionally, they collected related literature. This paper compiles the findings from that research.

Introduction

This author majored in architecture at university and, in the first year, mainly took foreign language and general education courses, in addition to some specialized architecture courses. These courses gave the author a strong sense of identity and joy as a student of architecture, and they were highly interesting. Among them, the most memorable was Professor Koichiro Kimura's course on "Architectural Health Engineering." In this course, Professor Kimura's book *The Theory of Architectural Planning* was used as the textbook.

Part of the course covered the German public health scholar Max von Pettenkofer. Pettenkofer was a professor at the University of Munich, and due to his popularity, many students attended his lectures. At that time, Munich winters were extremely cold, and the lectures were held with the windows tightly closed, which led to some students falling ill. Pettenkofer saw this as a decline in indoor air quality and attempted to measure the concentration of carbon dioxide. At that time, there were no gas analyzers, so lime was used to detect carbon dioxide. Through his research, he discovered that while carbon dioxide itself is not directly harmful to the human body, an increase in its concentration leads to a rise in harmful substances such as carbon monoxide and odors. He proposed that ventilation is necessary when the carbon dioxide concentration exceeds 1000 ppm. This standard is now widely accepted as a ventilation guideline.

Through this course, the author was deeply impressed by Pettenkofer's extraordinary insight and became eager to learn more about his achievements.

In July 2024, the author went to Munich to learn more about Max von Pettenkofer. The author found considerable evidence there of the general public's high regard for Pettenkofer. One piece was a statue of Pettenkofer in the center of Munich. Another was a major thoroughfare named after Pettenkofer. Yet another was how well kept was the gravesite of Pettenkofer, with greenery and fresh flowers.

The author visited the Max von Pettenkofer Institute, located within the University of Munich. This institute, which was founded by Pettenkofer, is a research center for public health and currently focuses on infectious diseases such as Covid-19. The author was told that the institute is especially busy with research on new infectious diseases from Africa. Finally, the institute introduced the author to books about Pettenkofer.

1. Max von Pettenkofer: From Uncertainty to a Scientific Methodology in Public Health"

Finally, the opportunity to utilize his practical and applicable scientific knowledge arrived. Max Gruber, in his eulogy for Max von Pettenkofer, stated the following:

"Until about the age of 40, he spent his time without progressing toward a clear goal. He devoted his great talents to many tasks without a plan. However, when he was given the right opportunity, he was able to utilize those talents and develop a scientific methodology. "radually, it became apparent that his seemingly sporadic activities over the past ten years were actually converging into a coherent purpose—to apply the knowledge and methods of natural science to public health. "The turning point in Pettenkofer's life was his investigation of a cholera outbreak in Munich. Through this research, he realized that he had begun to promote "the application of precise natural sciences, which had been scarcely practiced until then." Systematic investigations into people's living conditions and the scientific reassessment of public health were expected to yield richer results, in contrast to the traditional, experience-based approaches. His lectures also gradually changed, initially teaching chemistry but eventually expanding to cover the fields of "health management" and "medical policy."

Figure-1 The statue of Pettenkofer located in the center of Munich

Figure-2 Max von Pettenkofer Institute, University of Munich

Figure-3 A major road named after Pettenkofer in Munich

However, after engaging in debates about the causes of infectious diseases, Pettenkofer returned in 1851 to his research on indoor air quality. A committee to investigate ventilation in general hospitals was composed of professors from the university and technical university.

There was a committee chaired by Dr. Jolly, with Drs. Kaiser, Alexander, and Pettenkofer participating. Dr. Pettenkofer, based on his expertise in air quality at the royal palace, was tasked with investigating a specific ventilation system. He first conducted a thorough inspection of the new hospital building and began his "Observations on the Progress of Ventilation" on April 1, 1857.

As a result, although the ventilation system introduced by former director and an excellent architect, Heberl, was highly regarded as effective, it was found to be unsustainable in actual use. According to Pettenkofer's airflow measurements, the exchange of indoor and outdoor air occurred as expected in only 58 out of 100 instances, with the air flowing in the opposite direction in the remaining 42 instances.

Pettenkofer attempted to improve the ventilation, but he ultimately concluded that the system did not function at all. Furthermore, he sarcastically reported that the attending physician had opposed his findings, promoting the "improvement of the stove" as an expensive treatment.

During the hospital visits, the physicians ventilated the rooms using regular airflow to deceive the committee members into thinking it was the result of technical improvements in the ventilation system.

Regarding the progress of the investigation, Pettenkofer stated, "Since it became evident that the ventilation system could not be maintained, the committee, based on the chairman's suggestion, decided to send me to Paris, where I conducted a detailed comparative study on the latest ventilation systems." According to the 1858 report of the Royal Bavarian Academy of Sciences, the investigation in Paris was carried out with great rigor.

2. Pettenkofer and the Advancements in Hospital Ventilation: A Comparative Study of Traditional and Mechanical Systems

Pettenkofer delegated the task of investigating the ventilation system of the general hospital, assigned by the committee, to his disciple Georg Veichtinger during his absence from April to June 1857. Like Pettenkofer, Veichtinger found that, "the inflow of fresh air was somewhat more stable than in the maternity ward, but the discharge of polluted air was extremely inadequate," and he was disappointed with the results. During this time, Pettenkofer was studying the ventilation systems at La Riboisière Hospital and Beaujon Hospital in Paris, both of which had been installed based on thorough prior planning. Both ventilation systems were installed following a thorough preliminary examination to ensure the efficient exchange of air in the room. At La Riboisière Hospital, instead of relying on the conventional method of ventilation driven by the temperature difference between outside air and the indoor environment, a mechanical system powered by a steam engine was introduced. This system not only operated a centrifugal fan to circulate indoor air but also incorporated a hot water heating unit. After comparing this system with the traditional temperature-difference ventilation system, the hospital concluded that the airflow generated by mechanical ventilation was more uniform and superior.

Pettenkofer added his own sensory observations. In the conventional ventilation system, the smell of patients' sweat permeated the wards, whereas with the mechanical ventilation system, fresh air was evenly supplied, significantly improving the quality of the air. He also measured that, while the concentration of carbon dioxide in the traditional system was 2.5%, it dropped to 1% in the rooms with mechanical ventilation.

His impressions from La Riboisière Hospital highlighted several important points. First, he calculated the costs of the different systems and recognized that the mechanical ventilation system was considerably more expensive. In his paper, Pettenkofer used the term "hygiene," and he was convinced that the mechanical ventilation system was the most hygienic. However, he also noted that reducing costs and finding a more affordable and simpler way to operate the system would be a challenge for the future.

Furthermore, at the Beaujon Hospital in Paris, Pettenkofer discovered an intricate ventilation system designed by the Belgian engineer Van Hecke. This system broke away from the traditional principles of natural ventilation, instead

mechanically controlling air exchange. The heated air, as needed, was properly warmed through a tank, following the principles outlined in Pettenkofer's own research.

3. The Air Hygiene Research of Pettenkofer: Carbon Dioxide Measurement and Measures for Improving Living Environments

"The heated air needed to pass over the water tank. This was not only to warm the air but also to moderately humidify it. Pettenkofer was greatly impressed by this Van Hecke system and recommended it as the 'best method' during the construction of the new hospital in Augsburg.

Furthermore, Pettenkofer developed a method to accurately measure the concentration of carbon dioxide in the air using a device that absorbed carbon dioxide with limewater. In addition to this, he raised fundamental issues concerning 'good air in dwellings' at the Academy's Committee on Natural Science and Technology. This view was published in March 1858 and was groundbreaking in the field of air hygiene. The paper outlined the standards for good air and how it could be maintained through natural or artificial ventilation.

Pettenkofer focused on the quality of air in living spaces, once again emphasizing the importance of smell. 'It is the sense of smell that detects foreign substances in the air. The sense of smell can detect substances that cannot be identified by physical or chemical means. If the air causes discomfort to our sense of smell, it is thought to contain foreign substances. Pure air does not have such a sense of foreignness.' Therefore, while sufficient ventilation could be a solution, Pettenkofer also added the condition: 'as long as there is no source of air pollution.' For example, even if a hospital room or dining hall is ventilated, if poorly designed toilets constantly leak waste, the ventilation is compromised. Pettenkofer concluded that "hygiene cannot be maintained in places where perishable substances are not promptly removed or properly contained." Therefore, this is as follows: Max von Pettenkofer's lecture on hygiene at Ludwig Maximilian University: Max von Pettenkofer gave a lecture on hygiene during the summer semester of 1865 at Ludwig Maximilian University. The content of this lecture has been recorded. This was a topic Pettenkofer was particularly interested in and wished to communicate to the students of that time. The content of the lecture has been translated from the literature and is reproduced here.

1. Chemical composition of the atmosphere
2. Physical changes in the atmosphere and climate
3. Hygiene management of clothing and skin
4. Properties of building materials in relation to air and heat
5. Ventilation
6. Heating
7. Lighting
8. Building sites and foundations
9. Groundwater
10. Relationship between ground conditions and the occurrence and spread of specific diseases (malaria, typhoid fever, cholera), as well as the influence of local climate
11. Supply of drinking water and delivery systems to residential areas
12. Main components of food
13. Milk
14. Meat
15. Bread
16. Vegetables, fruits, and other plant-based foods
17. Low-alcohol beverages and vinegar
18. Condiments (salt, sugar, spices, tea, coffee, tobacco, etc.)
19. Nutrition and supply according to various social classes and conditions—supply regulations
20. Collection and disposal of excreta and other household waste, industrial waste—sewage treatment
21. Disinfection
22. Food inspection
23. Industries and factories harmful to health
24. Schools, barracks, welfare facilities, hospitals, gathering places
25. Preventive measures for toxic substances and their trade and distribution
26. Medical statistics—biostatistics

5.Conclusion

Max von Pettenkofer was born on December 3, 1818, in Lichtenheim, a suburb of Neuburg along the banks of the Danube River. When cholera spread across Europe, Pettenkofer took action to combat the epidemic. At that time, household waste was commonly disposed of in the soil. Pettenkofer argued that soil contamination was the cause of cholera and also claimed that polluted well water was a source of the disease. As he was a chemist rather than a physician, his views were met with fierce opposition from the medical community. He also advocated for the importance of building ventilation. In an era without gas analyzers, Pettenkofer used lime to measure carbon dioxide levels. He asserted that ventilation became necessary when CO_2 levels exceeded 1,000 ppm. While carbon dioxide itself is harmless to humans, he argued that an increase in CO_2 levels would lead to higher concentrations of harmful carbon monoxide and unpleasant odors.

In his younger years, Pettenkofer faced many challenges, often clashing with those who held different opinions. However, in his later years, he earned the trust of King Ludwig II, leading efforts to introduce a modern water supply and sewer system in Munich. As a result, the cholera outbreaks were brought under control, and Pettenkofer came to be known as the father of public health. After two cholera outbreaks in Munich in 1836 and 1854, Max von Pettenkofer was commissioned to study the causes and methods of cholera transmission. It was only after further outbreaks (typhus in 1872 and cholera in 1873/74) that the municipal magistrate of Munich seriously addressed the

renovation of the water supply and sewage systems. From 1881 to 1883, a hillside catchment area was constructed near the Mühlthal for the city's water supply. The source of the Kasperlbach was initially captured. After the construction was completed, a monument was erected over the original spring in 1883. On May 1, 1883, the water supply system became operational. The hillside spring catchment area still supplies water to Munich today.

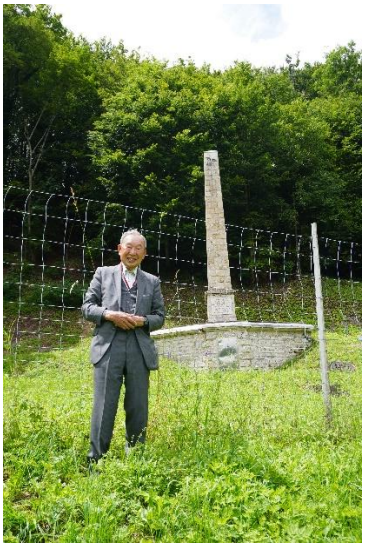

Figure-4 The commemorative obelisk erected at the water source, Kasperlbach, Mühlthal, where Pettenkofer installed the waterworks in Munich.

Figure-5 A plaque commemorating the introduction of the water supply to Munich

Acknowledgment

Pettenkofer gained the favor of Ludwig II in his later years and took advantage of this to advance his work. It seems that Mori Ōgai also studied under Pettenkofer and acquired knowledge, although his stay was relatively short. Ōgai wrote a short story about the discovery of Ludwig II's body in Starnberger See, titled "The Record of the Foam." In his later years, Pettenkofer too fell into darkness and took his own life in 1901.

I would like to express my gratitude to Dr. Helmut Künzel and Mr. Ziad Nouri for providing me with valuable literature on Max von Pettenkofer. I am also thankful to Ms. Yoko Rannmelmayr for guiding me to Pettenkofer's statue and to Ms. Eri Tanaka for showing me the water source that Pettenkofer's water system. Used to Munchi.

Figure-6 The grave of Pettenkofer surrounded by flowers , Munich

Figure-7 A cross standing at the location where the body of King Ludwig Ⅱwas found in Lake Starnberg.

References

1. Karl Kisskalt2Große Naturforscher, Band 4 , 「Max von Pttenkofer“Wissenschaftliche Verlagsgeselschaft M.B.H., Stuttgart 1948
2. Martin Weyer-von Schoultz, Max von Petenkofer (1818-1901), Peter Lang, Europäischer Verlag der Wissenschften
3. Karl Wieninger, Max von Pettenkofer, Ds Leben eines Wohltäters 1818-1901, Hugenduebel1987
4. Koichiro Kimura, Fundamentals of Architectural Planning.(Japanese)
5. Helmut Künzel, Bautraditionen auf dem Prüfstand, Fraunhofer IRB Verlag
6. Helmut Künzel, Richtiges Heizen und Lüften in Wohnungen, Fraunhofer IRB Verlag

A global synthesis of forest fire-related air pollution and its impact on public health

Student Member †Hadiwijoyo E (Tokyo City University)
Member Rijal H.B. (Tokyo City University)

Forest fires are increasingly recognized as significant contributors to global air pollution and public health burdens. This systematic review analyzes 14 peer-reviewed studies published between 2015 and 2025, focusing on the emissions and health consequences of wildfires across different regions. Emissions such as $PM_{2.5}$, CO_2, and VOCs were found to increase respiratory and cardiovascular mortality, particularly in vulnerable populations. Our findings highlight the need for improved fire management, air quality surveillance, and health interventions, especially in high-risk areas affected by recurring fire events. A transdisciplinary policy approach is urgently required to mitigate future risks.

1. Introduction

The frequency, intensity, and spatial extent of forest fires have escalated significantly from 2001 to 2019 across various biomes, including tropical, subtropical, temperate, and boreal ecosystems [1]. This trend is primarily driven by anthropogenic climate change and land-use alterations, positioning wildfires as a global environmental and public health crisis [2, 3]. These fires emit large volumes of fine particulate matter ($PM_{2.5}$), greenhouse gases, and toxic compounds such as polycyclic aromatic hydrocarbons (PAHs), often exceeding levels observed in industrialized urban centers [4, 5]. Wildfire emissions contribute to both short- and long-range atmospheric transport of pollutants, adversely impacting air quality hundreds to thousands of kilometers away [6, 7]. The resulting exposure is associated with increased morbidity and mortality, particularly from respiratory and cardiovascular conditions [8].

The degree of impact varies based on meteorological conditions, fire severity, vegetation type, and the socio-economic vulnerability of affected populations [9]. Integrative assessments reveal that biomass-burning emissions during major fire events can match, and in some contexts exceed, those from large urban centers, highlighting the necessity of coordinated air-quality monitoring and public health response strategies. Given that forest ecosystems themselves act as both sources and sinks of airborne pollutants, understanding the complex feedbacks between ecosystem health, atmospheric chemistry, and human well-being is essential for crafting effective mitigation and adaptation policies.

This paper presents a systematic literature review of peer-reviewed studies published between 2015 and 2025 in international journals (Scopus), focusing on the environmental and health consequences of wildfires. This literature review aims to examine emission components that affect human health and the environment. The ultimate goal is to inform fire Management policies and public health strategies through a better understanding of the complex interactions between wildfire, atmospheric pollution, and human well-being. Despite the growing number of studies, few reviews have integrated both environmental and health dimensions of wildfire impacts across diverse geographical settings in the last decade.

2. Methodology

A systematic literature review was conducted using the Scopus database to retrieve peer-reviewed articles. The search strategy employed the Boolean string: “forest AND fire AND air AND pollution AND human AND health”, targeting original studies that examined the direct environmental and/or health impacts of forest fires. Articles were included if they: (1) were written in English; (2) presented original quantitative findings; and (3) explicitly addressed pollutant emissions, human health outcomes, or both. Exclusion criteria encompassed: (1) reviews or meta-analyses; (2) studies unrelated to wildfire emissions; and (3) non-peer-reviewed publications. The initial search yielded 315 articles from the Scopus database. These articles were then screened based on title and abstract relevance. Eligible studies were those that explicitly examined either health outcomes (e.g., respiratory illnesses, mortality) or environmental impacts (e.g., air pollutant emissions), with a direct causal linkage to forest fire events. Articles were excluded if they focused on occupational exposure, indirect effects, or other non-fire-related pollution sources. Full-text screening led to the final selection of 14 eligible articles for in-depth analysis.

3. Results and discussion

3.1. Overview of selected studies

This review synthesizes empirical evidence on the impacts of forest fires on human health and environmental quality. These studies represent a diverse geographic scope, methodological approaches (modeling, epidemiological studies, field observations), and pollutant indicators ($PM_{2.5}$, CO, VOCs, etc.).

3.2. Impact on the environment

Wildfires and vegetation fires contribute significantly to atmospheric pollution, releasing a broad spectrum of

pollutants that vary by fuel type, fire intensity, and region. Table 1 summarizes findings from studies analyzing the environmental consequences of forest fire emissions.

Table 1. Summary of environmental impacts from wildfire-related emissions (2015–2025)

Reference	Location	Results
Zhang et al. [10]	Guangdong, China	OBB contributed 14% of total HCHO emissions; cropland fires emitted 26% more HCHO than forest fires.
Kaskaoutis et al., [11]	Athens, Greece	$PM_{2.5}$ ranged 8.9–78.7 μg/m³; 35.4 μg/m³ on active burning days.
Song et al. [12]	South China	2020 emissions: CO_2 = 30,568 Gg; $PM_{2.5}$ = 208 Gg.
Byrne et al. [13]	Canada	Total forest fire emissions reached 647 TgC, influenced by extreme heat conditions.
Zhang et al. [14]	Inner Mongolia, China	Highest $PM_{2.5}$ emissions linked to *Quercus mongolica*.
Wu et al.,[15]	Heilongjiang, China	*Betula platyphylla* bark yielded Emission Factor = 3.06 μg/m³.
Sutton et al.[16]	Yellowknife, Canada	Wildfires released 15–59% of global arsenic emissions.

Recent studies reveal that wildfire emissions not only rival but may even surpass anthropogenic sources such as transportation and industrial activities. For instance, Song et al. [12] and Byrne et al. [13] documented large-scale carbon-based emissions, highlighting the substantial role of fire-induced carbon fluxes in national greenhouse gas inventories. Forest fires significantly elevate ambient concentrations of fine particulate matter ($PM_{2.5}$); for instance, Kaskaoutis et al. [11] reported that $PM_{2.5}$ levels rose to 35.4 μg/m³ during active burning periods. This underscores the importance of understanding the specific drivers behind such emissions, including the type of fuel involved.

Fuel composition, in particular, plays a critical role in shaping emission profiles. Species such as Quercus mongolica and Betula platyphylla have been shown to emit disproportionately high levels of fine particulate matter during combustion [14, 15]. Adding another layer of concern, Sutton et al. [16] introduced a toxicological perspective by reporting significant arsenic emissions from wildfires in mining-impacted regions, thus linking biomass burning not only to air pollution but also to heavy metal contamination of surrounding ecosystems. Among various fire types, peatland fires represent an especially pressing concern in Southeast Asia due to their high organic content and smoke-producing potential. Fisher et al. [17] estimated that during extreme haze events, peatland fires contributed approximately 10% of global particulate matter emissions. These emissions are not only persistent but also hazardous, posing long-term threats to regional air quality and public health.

In general, these findings highlight the urgent need for region-specific fire monitoring systems, detailed fuel-type characterization, and the integration of wildfire dynamics into both national air quality management and international climate mitigation policies. A comprehensive understanding of the ecological and chemical complexity of wildfire emissions, particularly from peatlands and species with high particulate yields, is essential for developing effective strategies to mitigate their environmental and health impacts.

3.3. Impact on human health

The health consequences of wildfire smoke are increasingly documented, with exposure linked to respiratory infections, cardiovascular complications, and premature mortality. Table 2 presents evidence from selected studies that quantified health outcomes associated with forest fire exposure.

Studies in developed countries such as the United States and Australia show consistent associations between wildfire exposure and adverse health outcomes. Pye et al. [18] reported that the oxidative potential of wildfire-derived PM, particularly from Reactive Organic Compounds (ROCs), constitutes the main driver of toxicity. Wen et al. [19] further emphasized that health impacts are disproportionately distributed, with low-income populations experiencing heightened vulnerability due to limited adaptive capacity and poor healthcare access.

In contrast, studies in Thailand, such as Pongpiachan et al. [20], found relatively lower associations between biomass burning and PAH-related health burdens. This variability may be due to differences in combustion efficiency, local biomass composition, and existing background air pollution. However, in Indonesia, an estimated 648 premature deaths occur each year, equivalent to 26 deaths per 100,000 population, mainly driven by elevated concentrations of $PM_{2.5}$, which are linked to chronic respiratory disorders, cardiovascular diseases, and lung cancer [21, 22].

Evidence from Brazil [23] and Portugal [24] suggests that repeated exposure during peak fire years is linked not only to mortality but also to long-term health system strain and economic losses. These findings reinforce the need to incorporate wildfire smoke as a formal determinant of public health within national disease surveillance systems. Overall, forest fires represent a significant public health concern, as they can contribute to human mortality both directly and

indirectly. This is primarily due to the inhalation of toxic gases and fine particulate matter released during combustion processes. Such exposures are often unrecognized in real time but may lead to severe respiratory and cardiovascular outcomes. Consequently, effective fire prevention strategies are essential to minimize the release of hazardous emissions and protect human health.

Table 2. Summary of human health effects associated with forest fire emissions

Reference	Location	Results
Tarín-Carrasco et al.[25]	Portugal	35% increase in respiratory mortality during fire years.
Pye et al. [18]	Western USA	Emissions: 1250 g ROC/kg CO; particulate phase drives health burden.
Wen et al. [19]	New South Wales, Australia	Higher health risk in low socioeconomic status and high fire-density areas.
Pongpiachan et al.[20]	Northern Thailand	Minor role of PAHs from biomass burning in local health effects
Maji et al.[21]	Southeastern USA (10 states)	$PM_{2.5}$ increased by 10% (prescribed) and 22% (extensive burns); mortality linked.
Schroeder et al. [23]	Brazil	Strong Spearman correlation (r_s = 0.66) between fire events and respiratory death.
Barbosa et al.[24]	Portugal	High wildfire emissions in 2017 coincided with increased mortality and economic loss.

3.4 Policy implications and cross-regional comparisons

The reviewed evidence underscores a critical policy gap in integrated fire management, especially across low- and middle-income countries. While countries such as the U.S. and Australia have advanced early warning and air monitoring systems, many regions in Southeast Asia and South America lack robust infrastructure to track, mitigate, and respond to fire-related health threats [26].

Moreover, wildfire emissions, though largely treated as episodic events, are now chronic contributors to poor air quality in many regions. The transboundary nature of wildfire impacts further exacerbates the problem, affecting neighboring areas and even distant countries. This necessitates a shift in environmental governance, wherein wildfires are treated as both a climate resilience and public health issue.

We recommend:

1. Prioritizing community-level early warning systems and temporary shelters with clean air access in fire-prone zones;
2. Enhancing health surveillance systems to detect spikes in respiratory/cardiovascular cases following large fire events.
3. Integrating fire management policies across sectors and regions, including through regional agreements to address transboundary impacts.
4. Promoting long-term investment in emission and air quality monitoring infrastructure to support evidence-based mitigation.

4. Conclusions

Forest fires are a growing environmental health concern, with wide-ranging impacts on air quality, ecosystem integrity, and public health. The reviewed literature highlights consistent associations between wildfire emissions and adverse health outcomes, particularly respiratory and cardiovascular morbidity and mortality.

Given the projected rise in wildfire frequency and severity under climate change, urgent action is required. Policies must integrate fire prevention, real-time pollution monitoring, and targeted health interventions for at-risk populations. A multidisciplinary approach—combining environmental science, public health, and disaster preparedness is essential to address the escalating risks posed by forest fires globally.

Acknowledgments

The work was supported by the Ministry of Education, Culture, Sports, Science and Technology (Monbukagakusho) of Japan for the financial support provided through the MEXT Scholarship Program.

References

[1] Tyukavina, A., Potapov, P., Hansen, M. C., Pickens, A. H., Stehman, S. V, Turubanova, S., Parker, D., Zalles, V., Lima, A., Kommareddy, I., Song, X.-P., Wang, L., & Harris, N. (2022). Global trends of forest loss due to fire from 2001 to 2019. *Frontiers in Remote Sensing*, 3(825190).

[2] Jones, M. W., Abatzoglou, J. T., Veraverbeke, S., Andela, N., Lasslop, G., Forkel, M., Smith, A. J. P., Burton, C., Betts, R. A., van der Werf, G. R., Sitch, S., Canadell, J. G., Santín, C., Kolden, C., Doerr, S. H., & Le Quéré, C. (2022). Global and regional trends and drivers of fire under climate change. *Reviews of Geophysics*, *60*(3), e2020RG000726.

[3] Sengupta, S., Aneja, V. P., & Kravchenko, J. (2022). *Wildfire pollution exposure and human health: a growing air quality and public health issue*. *Environmental Sciences Proceedings.* 2022, 19,59.

[4] Sahu, R. K., Hari, M., & Tyagi, B. (2022). Forest fire

induced air pollution over Eastern India during March 2021. *Aerosol and Air Quality Research*, *22*(8): 220084

[5] Jerrett, M., Jina, A. S., & Marlier, M. E. (2022). Up in smoke: California's greenhouse gas reductions could be wiped out by 2020 wildfires. *Environmental Pollution*, *310* (119888)

[6] Lapere, R., Mailler, S., & Menut, L. (2021). The 2017 mega-fires in central chile: Impacts on regional atmospheric composition and meteorology assessed from satellite data and chemistry-transport modeling. *Atmosphere*, *12*(3), 12030344

[7] Adame, J. A., Lope, L., Hidalgo, P. J., Sorribas, M., Gutiérrez-Álvarez, I., del Águila, A., Saiz-Lopez, A., & Yela, M. (2018). Study of the exceptional meteorological conditions, trace gases and particulate matter measured during the 2017 forest fire in Doñana Natural Park, Spain. *Science of the Total Environment*, *645*(2), 710–720.

[8] Ranse, J., Luther, M., Hertelendy, A., & Skinner, R. (2022). Impact of fine particulate matter ($PM_{2.5}$) smoke during the 2019 / 2020 Australian bushfire disaster on emergency department patient presentations. *Journal of Climate Change and Health*, *6* (100113).

[9] de Diego, J., Rúa, A., & Fernández, M. (2021). Vulnerability variables and their effect on wildfires in galicia (Spain). A panel data analysis. *Land*, *10*(10).

[10] Zhang, C., Li, J., Zhao, W., Yao, Q., Wang, H., & Wang, B. (2022). Open biomass burning emissions and their contribution to ambient formaldehyde in Guangdong province, China. *Science of the Total Environment*, 838 (155904).

[11] Kaskaoutis, D. G., Petrinoli, K., Grivas, G., Kalkavouras, P., Tsagkaraki, M., Tavernaraki, K., Papoutsidaki, K., Stavroulas, I., Paraskevopoulou, D., Bougiatioti, A., Gerasopoulos, E., & Mihalopoulos, N. (2024). Impact of peri-urban forest fires on air quality and aerosol optical and chemical properties: The case of the August 2021 wildfires in Athens, Greece. *Science of the Total Environment*, *907* (168028).

[12] Song, R., Wang, T., Han, J., Xu, B., Ma, D., Zhang, M., Li, S., Zhuang, B., Li, M., & Xie, M. (2022). Spatial and temporal variation of air pollutant emissions from forest fires in China. *Atmospheric Environment*, *281* (119156).

[13] Byrne, B., Liu, J., Bowman, K. W., Pascolini-Campbell, M., Chatterjee, A., Pandey, S., Miyazaki, K., van der Werf, G. R., Wunch, D., Wennberg, P. O., Roehl, C. M., & Sinha, S. (2024). Carbon emissions from the 2023 Canadian wildfires. *Nature*, *633*(8031), 835–839.

[14] Zhang, H., Li, H., Liu, X., Ma, Y., Zhou, Q., Sa, R., & Zhang, Q. (2022). Emissions Released by Forest Fuel in the Daxing'an Mountains, China. *Forests*, *13*(8).

[15] Wu, Z., Hasham, A., Zhang, T., Gu, Y., Lu, B., Sun, H., & Shu, Z. (2024). Analysis of $PM_{2.5}$ concentration released from forest combustion in Liangshui National Natural Reserve, China. *Fire*, *7*(9).

[16] Sutton, O. F., Mccarter, C. P. R., & Waddington, J. M. (2024). *Globally-significant arsenic release by wildfires in a mining-impacted boreal landscape*. E*nvironmental Research Letters* 19 (064024).

[17] Fisher, D., Wooster, M. J., Xu, W., Thomas, G., & Lestari, P. (2020). Top-down estimation of particulate matter emissions from extreme tropical peatland fires using geostationary satellite fire radiative power observations. *Sensors, 20*(24).

[18] Pye, H. O. T., Xu, L., Henderson, B. H., Pagonis, D., Campuzano-Jost, P., Guo, H., Jimenez, J. L., Allen, C., Skipper, T. N., Halliday, H. S., Murphy, B. N., D'Ambro, E. L., Wennberg, P. O., Place, B. K., Wiser, F. C., McNeill, V. F., Apel, E. C., Blake, D. R., Coggon, M. M., Crounse, J. D., Gilman, J. B., Gkatzelis, G. I., Hanisco, T. F., Huey, L. G., Katich, J. M., Lamplugh, A., Lindaas, J., Peischl, J., Clair, J. M. S., Warneke, C., Wolfe, G. M., and Womack, C. (2024). Evolution of reactive organic compounds and their potential health risk in wildfire smoke. *Environmental Science and Technology*, *58*(44), 19785 – 19796.

[19] Wen, B., Wu, Y., Xu, R., Guo, Y., & Li, S. (2022). Excess emergency department visits for cardiovascular and respiratory diseases during the 2019 – 20 bush fi re period in Australia : A two-stage interrupted time-series analysis. *Science of the Total Environment*, *809*(152226).

[20] Pongpiachan, S., Tipmanee, D., Khumsup, C., Kittikoon, I., & Hirunyatrakul, P. (2015). Assessing risks to adults and preschool children posed by $PM_{2.5}$-bound polycyclic aromatic hydrocarbons (pahs) during a biomass burning episode in Northern Thailand. *Science of the Total Environment*, *508*, 435 – 444.

[21] Maji, K. J., Li, Z., Hu, Y., Vaidyanathan, A., Stowell, J. D., Milando, C., Wellenius, G., Kinney, P. L., Russell, A. G., & Talat Odman, M. (2024). Prescribed burn related increases of population exposure to $PM_{2.5}$ and O3 pollution in the southeastern US over 2013–2020. *Environment International*, *193*.

[22] Uda, S. K., Hein, L., & Atmoko, D. (2019). Assessing the health impacts of peatland fires: a case study for Central Kalimantan, Indonesia. *Environmental Science and Pollution Research*, *26*(30), 31315–31327.

[23] Schroeder, L., Veronez, M. R., de Souza, E. M., Brum, D., Gonzaga, L., & Rofatto, V. F. (2020). Respiratory diseases, malaria and leishmaniasis: Temporal and spatial association with fire occurrences from knowledge discovery and data mining. *International Journal of Environmental Research and Public Health*, *17*(10).

[24] Barbosa, J. V, Nunes, R. A. O., Alvim-Ferraz, M. C. M., Martins, F. G., & Sousa, S. I. V. (2024). Health and economic burden of wildland fires $PM_{2.5}$-related pollution in Portugal – A longitudinal study. *Environmental Research*, *240*, (117490).

[25] Tarín-Carrasco, P., Augusto, S., Palacios-Penã, L., Ratola, N., & Jiménez-Guerrero, P. (2021). Impact of large wildfires on PM10 levels and human mortality in Portugal. *Natural Hazards and Earth System Sciences*, *21*(9), 2867–2880.

[26] Verma, R. L., Oanh, N. T. K., Winijkul, E., Huy, L. N., Armart, I. P., Laowagul, W., Sooktawee, S., Permadi, D. A., Khan, M. F., Gunawardhana, L., & Patdu, M. K. (2023). Air quality management status and needs of countries in South Asia and Southeast Asia. *APN Science Bulletin*, *13*(1), 130–152.

Impact of the heat transfer mechanism of personal comfort systems on thermal comfort and energy performance

Student Member †Arachchi A.P.D.T. (Tokyo City University)
Member Rijal H.B. (Tokyo City University)

Personal comfort systems (PCS), which provide targeted heating or cooling to specific body parts, have emerged as a promising solution to enhance occupant comfort while reducing energy use in buildings. This study investigates the impact of heat transfer mechanisms (HTM) such as conduction, convection, and radiation of the PCS on thermal comfort improvement and energy performance in both heating and cooling modes. It addresses a critical gap in understanding optimal HTMs of PCS to achieve thermal comfort and energy efficiency. A meta-analysis was conducted, extracting data from 64 previous studies to evaluate the effects of HTMs of PCS on thermal sensation votes (*TSV*), overall comfort (*OC*) and corrective energy power (*CEP*, W/°C). Results indicate that simultaneously use of several HTMs improve thermal perception higher compared to one HTM alone for both heating and cooling modes. Convection was found to be the most efficient HTM for cooling while conduction is the most efficient for heating mode. Oppositely, Radiation for cooling and convection for heating were found to be the least efficient HTMs. Most of the HTMs consume less than 100 W per 1 °C improvement in perception. These findings underscore the potential of carefully selecting HTMs in PCS for achieving maximum thermal comfort with significant energy savings.

1. Introduction

High energy consumption in buildings remains a critical global challenge and it is approximately about 30% of global energy consumption [1]. Heating, ventilation and air conditioning (HVAC) systems are consuming about half of total building energy usage [2]. HVAC systems typically achieve thermal comfort satisfaction for approximately 80% of occupants [3]. Integration of Personal comfort systems (PCS) has shown significant improvements in occupant satisfaction and energy savings [4,5].

Heat transfer mechanism (HTM) plays a critical role in shaping the effectiveness of PCS by influencing thermal perception and energy efficiency [5]. There was a critical gap found in literature in understanding the HTMs impact on comfort performance of PCS [6]. Therefore, this study aims to explore the impact of HTM on thermal comfort and energy performance of PCS in both heating and cooling modes by conducting a meta-analysis across previous studies.

2. Methodology

Data were collected from original PCS studies following meta-analysis methodologies [7]. Through a Scopus database search, 64 research articles were selected for this study [20]. Heating and cooling devices classified according to Song et al [8], whole body thermal sensation vote (*TSV*) and overall comfort (*OC*) values in same indoor air temperature were extracted for conditions with PCS and without PCS. At the same time, power (W) values of the PCS at the relevant indoor was collected In cases where exact TSV and OC values were not provided in text, *TSV* and *OC* graphs were utilized for data extraction and LabPlot software [9] was employed to record data points. Measured *TSV* and *OC* values were following ASHRAE 7-point scale. Some data points were not included, as it was hard to identify whether the heating or cooling mode of PCS was activated during the survey.

2.1. Classification of *HTM*

Devices that come into direct contact with the subject's skin for heating or cooling purposes were classified as conductive (*Cd*) devices, those that stimulate the surrounding air to provide thermal comfort are categorized as convective (*Cv*) devices and devices that do not make direct contact with the body, do not influence the surrounding air, and provide heating solely through radiation are considered radiative (*Rd*) devices for this study following Song et al. [8]. When the PCS studies employed several HTMs simultaneously it was categorized separately considering as a distinct HTM such as *Cd & Cv, Cd & Rd, Cd & Rd* and *Cd, Cv & Rd*.

2.2. Thermal comfort performance

To measure thermal comfort performance, this study used the difference of TSV (ΔTSV) and OC (ΔOC) made by PCS at same indoor air temperature. This indicates how much change in thermal perceptual responses is made by PCS in particular thermal environment. ΔTSV and ΔOC were calculated using following equations.

$$\Delta TSV = TSV_{With\ PCS} - TSV_{Without\ PCS} \quad (1)$$

$$\Delta OC = OC_{With\ PCS} - OC_{Without\ PCS} \quad (2)$$

2.3. Energy performance

To measure energy efficiency of PCS in achieving thermal comfort for occupants, corrective energy power (*CEP,* W/°C) is the widely used parameter in PCS studies. *CEP* is defined as the quantification of power needed for adjusting an individual's thermal perception towards comfortable perception by particular heating or cooling PCS [10,11]. To

eliminate abnormal results, absolute *CEP* was used for analysis, and it was calculated using following equation.

Absolute $CEP = P / (\text{Absolute } \Delta TSV / G)$ (3)

Where P is Power value of the PCS device and G is Griffiths' constant. G is assumed to be 0.33.

3. Results and discussion

3.1. Data availability

Among the data collected from 64 PCS studies, the HTMs were not equally distributed, and for some HTMs there was no data available in literature as shown in Table 1 *Cd* and *Cv* HTMs have the highest number of data while *Rd* has a lower amount of data. All other combined HTMs have a very few data. Previous studies have not studied employing several HTMs simultaneously in PCS broadly and many studies have not provided the power values of the studied PCS. These results indicate the importance of focusing studies into combined HTMs in PCS.

Table 1 Number of data included for this study for each heat transfer mechanism

Heat Transfer Mechanism	Number of data for *TSV*		Number of data for *OC*		Number of data for *CEP*	
	Heating	Cooling	Heating	Cooling	Heating	Cooling
Cd	156	40	149	39	27	144
Cv	16	192	13	151	73	2
Rd	22	8	15	8	2	19
Cd & Cv	4	9	4	9	6	
Cd & Rd	10	-	10	-	-	10
CV & Rd	8	6	8	6	-	
Cd, Cv & Rd	4	-	4	-	-	4
Total	220	255	203	213	108	179

3.2. Impact of PCS on perceptual responses

Perceptual responses are important for measuring human thermal comfort. *TSV* provides a measurement on how people feel at certain environment [12] while *OC* offering a more accurate measure of comfort accumulating with the combined effects of other environmental factors [13,14].

The *TSV* and *OC* have positive and negative values. While obtaining the differences of those values (ΔTSV and ΔOC) for analyzing the impact done by PCS precisely, negative values might be abnormal. Therefore, only absolute differences of *TSV* and *OC* values of those variables were considered for this study.

Table 2 Mean for with PCS, without PCS and absolute differences of *TSV* and *OC*.

Mode	TSV			OC		
	Without PCS	With PCS	Absolute Difference	Without PCS	With PCS	Absolute Difference
Heating	-0.84	-0.12	0.74	-0.42	0.52	0.96
Cooling	0.95	0.20	0.77	-0.05	0.72	0.72

Table 2 shows the mean values of *TSV* and *OC* for with and without PCS conditions with absolute ΔTSV and ΔOC done by the PCS. For both modes there are significant changes in mean *TSV* and *OC* found when using PCS and the improvement is about 1-point for both *TSV* and *OC* for both heating and cooling modes.

Fig.1 shows the distribution of absolute ΔTSV in cooling and heating modes. For both graphs, the general trend shows that most of the absolute ΔTSV are clustered around 0.7 relatively close to zero. However, the standard deviation indicated that there is still some variability in absolute ΔTSV made by different PCS in different environments.

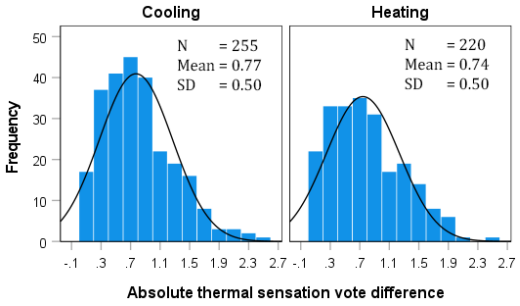

Figure 1 Distribution of absolute ΔTSV

Fig. 2 shows the distributions of absolute ΔOC in heating and cooling modes. In both cases, the highest frequencies were observed for lower absolute ΔOC values, indicating a general tendency for people to have similar overall comfort assessments when use PCS similar to *TSV*. However, the heating condition displays a slightly higher mean, and a larger standard deviation compared to cooling, suggesting greater variability in comfort perceptions under heating.

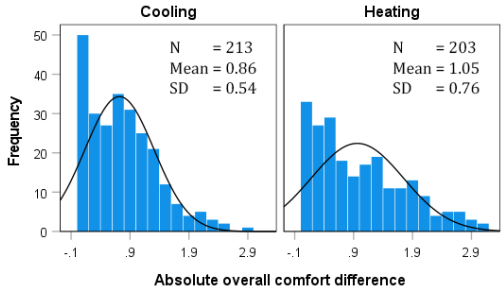

Figure 2 Distribution of absolute ΔOC

3.3. HTM's impact on thermal comfort

3.3.1. Impact on TSV

Thermal comfort performance of PCS depends on various factors and HTM is one of them [5]. Choosing an optimum HTM in PCS is crucial because it maximizes localized thermal comfort [6]. For this study ΔTSV and ΔOC done by the PCS were considered as thermal comfort performance of certain HTM of PCS.

Fig.3 shows the mean absolute ΔTSV for various heat transfer mechanisms under both cooling and heating conditions. For

most of the single HTMs (*Cd, Cv, Rd*), the mean absolute Δ*TSV* are generally around 0.75 and approximately similar, for both modes but *Rd* for cooling shows a significant lower value compared to other single HTMs. In combinations of HTMs, *Cd & Cv* and *Cv & Rd* show higher values compared to other HTMs for cooling mode. *Cd & Cv* and *Cd, Cv & Rd* and *Cd, Cv & Rd* show higher absolute Δ*TSV,* but *Cd & Rd* and *Cv & Rd* show lower values compared to other HTMs for heating mode. For example, the "*Cd, Cv, & Rd*" mechanism under heating has a very wide confidence interval. This may be due to the lack of data for those HTMs.

Even though some data shows higher uncertainties and variabilities, the results suggest that when PCS employ single HTMs, people tend to have more similar *TSV* improvements for all of the cases except *Rd* for cooling mode. Employing multiple HTMs simultaneously in PCS can improve constructively but for some mechanisms it works destructively. *Rd* for cooling and using *Rd* with *Cv* and *Cd* for cooling are less effective while *Cd* for heating and *Cv & Rd* for cooling are the best effective HTMs according to *TSV* data.

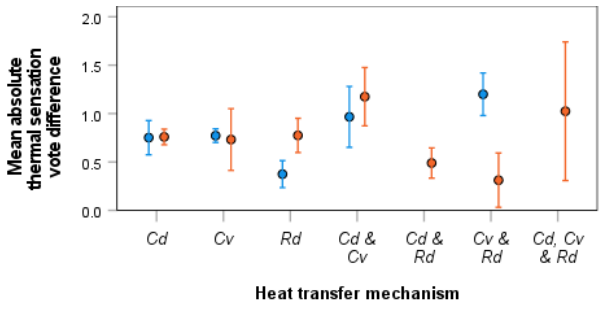

Figure 3 Mean absolute Δ*TSV* and 95% confidence interval (mean ± S.E.) for different HTMs

3.3.2. Impact on OC

Fig.4. illustrates the mean absolute Δ*OC* for various HTMs under heating and cooling modes. Similar to the *TSV*, the overall absolute Δ*OC* tend to be larger when multiple HTMs are involved for most of the cases for both heating and cooling. For single HTMs, the mean absolute Δ*OC* are generally smaller except *Cv* and *Cd* for heating. Combined HTMs show slightly higher absolute Δ*OC* improvements rather than most of single HTMs. *Cd, Cv & Rd* is the best effective HTM for heating mode while *Cd & Cv* is the best for cooling mode. Rd is the least effective for both heating and cooling modes according to *OC* data. The results suggests that combined HTMs can improve absolute Δ*OC* higher than single HTMs but when multiple HTMs are employed, absolute Δ*OC* likely lead to more diverse. *Cv* based HTMs are better for improving OC in heating mode while *Cd* based HTMs are better for cooling mode.

To determine the most effective heat transfer methodology comprehensively, the mean absolute changes in *TSV* and *OC* done by PCS in both heating and cooling modes were analyzed in this section. Comparing both *TSV* and *OC* data, The highest impactful HTMs for heating mode were *Cd, Cv & Rd* and *Cv* while *Cv* based combined HTMs were highest impactful for cooling modes. The least effective HTM was *Rd* for both heating and cooling mode. As single HTMs *Cd* in heating and *Cv* in cooling can improve thermal perception according to Δ*TSV* while *Cv* in heating and *Cd* in cooling can improve overall comfort perception according to Δ*OC*.

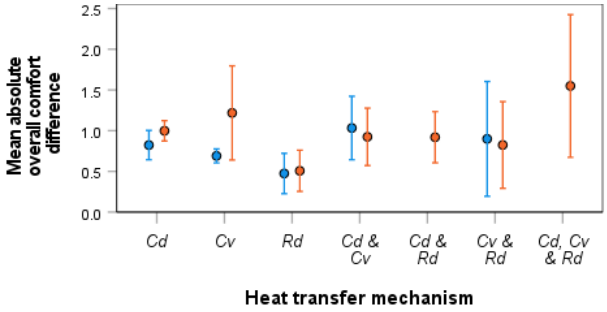

Figure 4 Mean absolute Δ*OC* and 95% confidence interval (mean ± S.E.) for different HTMs

3.3.1. Overall discussion

For the heating mode, Tang et al. [15] identified *Cd* as the most effective HTM for *OC* improvement, followed by *Cv* and *Rd*. For TSV, *Cv* was found to be the most effective, followed by *Cd* and *Rd*. However, Yang et al. [16] indicated that *Rd* was more effective for *OC* improvement, whereas *Cv* was more effective for TSV enhancement. Some other study suggested that *Rd* was the most effective HTM, followed by *Cv* and *Cd* [17]. Additionally, studies demonstrated that high power *Rd* could exceed *Cd*'s performance, while *Cd* was found to be more effective than *Cv* in heating PCS [6].

For cooling mode, other studies have identified *Cv* as highly effective HTM, particularly when fan-assisted airflow was employed. *Cv* significantly enhanced heat dissipation to the surrounding air. *Rd* was found to be effective in facilitating heat exchange when body temperature exceeded the ambient temperature. In contrast, *Cd* heat transfer was observed to be the least effective when applied alone, as it relied on direct contact with surfaces and influenced only limited areas of the body. However, its effectiveness was significantly enhanced when combined with other HTMs [18].

3.4. HTM's impact on energy performance

The energy use of PCS is important because it can significantly reduce the energy consumption of conventional HVAC systems by conditioning only occupied zones, leading to substantial energy savings while maintaining or improving occupant comfort [8]. The HTM used in PCS is crucial to energy consumption because employing more efficient modes can deliver targeted thermal comfort with significantly lower power use compared to conventional systems [6,19]. To

measure the energy consumption of the PCS by each HTM, this study analyzed the absolute *CEP* of PCS. This metric simply indicates the power (W) needed to improve the 1°C in thermal perception for a certain PCS.

Fig.5.shows the distribution of absolute *CEP* for both heating and cooling modes. It has skewed to the right, with most values concentrated between 0 and 100 W/°C for both modes. The absolute *CEP* values of heating mode are generally higher and more spread out than in the cooling mode and number of available data is higher in heating mode. This signifies that correcting thermal perception during heating typically requires more energy and is more variable compared to cooling mode but in most cases, only a small amount (<100 W/°C) of energy can improve thermal perception for both heating and colling modes.

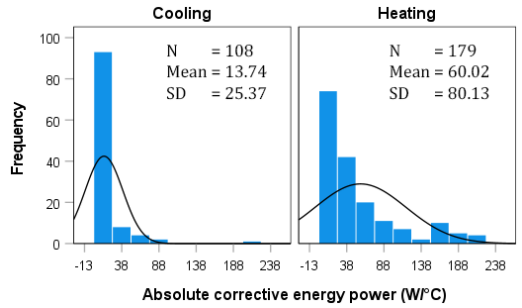

Figure 5 Distribution of absolute *CEP*

Fig. 6 displays the mean absolute *CEP* for various HTMs under both cooling and heating modes. The confidence intervals vary across HTMs and modes. This may be due to the lower number of available data for those HTMs (Table 1). In general, the absolute *CEP* tends to be higher for most of the HTMs of heating compared to cooling. *Cv* stands out with a substantially higher mean absolute *CEP* compared to other HTMs for heating mode while *Rd* is for cooling mode. *Cd* shows the lowest absolute *CEP* for heating mode and *Cv* shows the lowest for heating.

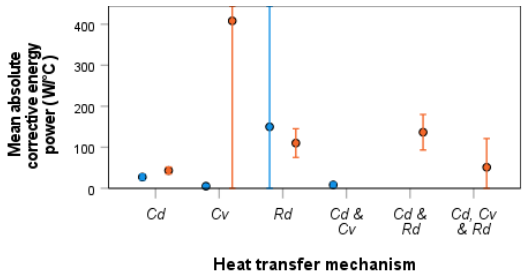

Figure 6 Mean absolute *CEP* and 95% confidence interval (mean ± S.E.) for different HTMs

Findings suggest that generally many HTMs of PCS consume more energy to modify thermal perception in heating mode than cooling mode. A large amount of energy is needed to improve comfort in *Cv* for heating mode and *Rd* for cooling mode. The most energy efficient HTM for cooling mode is *Cv* and *Cd* is for heating mode. Considering both comfort and energy performance *Cv* based HTMs for cooling mode and *Cd* based HTMs can be recommended to PCS for achieving maximum comfort and energy savings according to this meta-analysis results. Further studies and validation are needed using combined HTMs in PCS in different contexts.

4. Conclusions

Following results were found from this meta-analysis.

1. The uneven distribution of data across different heat transfer mechanisms, particularly for combined HTMs, underscoring the need for more studies on multiple HTMs to better understand their impact on PCS performance.
2. PCS significantly improves thermal sensation and overall comfort by approximately 1 scale unit in both heating and cooling modes.
3. *Cd* alone, *Cd, Cv & Rd* and *Cv* for heating mode while *Cv* based combined HTMs for cooling mode were highest effective HTMs while *Rd* was the least effective HTM for both heating and cooling modes.
4. Most of the PCS consume less energy (100 W/°C) to improve thermal perception in both modes while most of the HTMs in heating mode slightly higher values compared to cooling mode. *Cd* for heating and *Cv for* cooling are recommended as the most comfort improving and energy-efficient HTMs.

Acknowledgements

We acknowledge the authors whose research work has been reviewed in this paper. Their valuable studies and clearly stated insights have provided the foundation for this review.

References

1. IEA Tracking Report - Buildings | Global ABC
2. Energy in time | Project | CORDIS | European Commission
3. Kim et al. Build Environ. 2019; 148:348–360
4. Personal Comfort Systems | ashrae.org
5. Luo et al. Energy Build. 2022; 256:111766
6. Zhu et al. Build Environ. 2025; 268:112350
7. Sen & Yildirim. Psych. 2022;4(4):640–667
8. Song et al. Energy Build. 2022; 256:111747
9. LabPlot : https://labplot.org/
10. He et al. Build Environ. 2017; 112:285–295
11. Liu et al. Build Environ. 2024; 257:111532
12. Aqilah et al. Energies. 2022;15(23)
13. Peddie et al. Aust J Multi-Discip Eng. 2020;16(1):20–30
14. Lian. Build Simul. 2024;17(2):185–8
15. Tang et al. Build Environ. 2022;217.109069
16. Yang et al. Build Environ. 2024; 247:111004
17. Yang et al. Buildings. 2024;14(12).
18. Enescu. Energies. 2024;17(2):285
19. Rugani et al. Build Environ. 2023; 244:110787
20. Arachchi APDT (2025). Previous Personal Comfort Systems Studies [Data set]. Zenodo. https://doi.org/10.5281/zenodo.15100660

Numerical Modeling of Monkey Upper Airways for Inhalation Exposure Assessment Compared to Human Characteristics

Student Member †Yuichiro SUDA (Kyushu University) Member Kazuki KUGA (Kyushu University) Member Kazuhide ITO (Kyushu University)

This study developed numerical airway models of Japanese macaques (*Macaca fuscata*) using CT data to assess inhalation exposure and compared their particle transport characteristics with those of humans. Simulations revealed that macaques maintained high aspiration efficiency for particles up to 10 μm, with deposition patterns similar to those of humans. Age and body weight influenced individual differences in particle deposition, particularly for larger particles. These findings highlight the utility of macaque models for evaluating airborne infection risks and provide insights into interspecies differences that are essential for improving extrapolation from animal studies to human health assessments.

1. Introduction

Recent viral infections have had a profound global impact, primarily by spreading through airborne micro-particles. Understanding airflow and particle transport dynamics within the airway, particularly through the nasal passage, is a critical challenge in biofluid engineering. Owing to ethical constraints on human studies, inhalation exposure assessments predominantly rely on data from experimental animals. However, accurate extrapolation to humans necessitates a precise understanding of the interspecies physiological differences that remain insufficiently explored. Among non-human primates (NHPs), the Japanese macaque (*Macaca fuscata*) serves as a valuable human analog; however, its airway particle transport characteristics require further investigation.

In this study, we constructed numerical airway models for multiple Japanese macaques (*Macaca fuscata*) by reconstructing the detailed geometry of the upper airway, from the nasal cavity to the trachea, based on computed tomography (CT) data. We performed computational fluid particle dynamics (CFPD) simulations to analyze inhaled particle transport and deposition during steady breathing across individuals and humans. Using this approach, we demonstrated the utility of primate-based particle transport and deposition analysis as a methodology for assessing aerosol infection risks.

2. Methods

2.1. CFD monkey models and numerical solutions

Geometric monkey models were constructed based on CT data. In this study, the numerical monkey model included not only the upper airway from the nostrils to the trachea but also the facial morphology and an external breathing zone (Fig. 1). The geometry was segmented using the ANSYS Space Claim

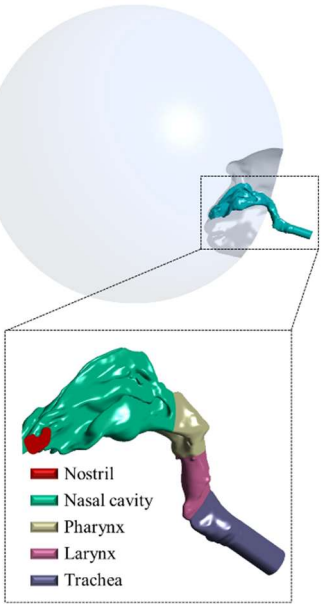

Figure-1 Computational monkey airway model (PRI-Mff765).

software to enable interindividual comparisons. ANSYS Fluent (2023R2, ANSYS Inc.) was employed for the fluid and particle simulations. The Reynolds-averaged Navier-Stokes equations were solved to predict the steady-state airflow, using the shear stress transport (SST) k-ω turbulence model. This analysis imposed a velocity boundary condition at the tracheal outlet to simulate the pulling airflow motion, following Karel et al. [1]. The minute volume (MV) was calculated using the following equation:

$$MV = TV \times BW \times RR \quad (1)$$

where TV is the tidal volume (10.1 mL/kg), BW is body weight, and RR is the respiratory rate (37 breaths/min). The detailed parameters for each individual are listed in Table 1.

2.2. Methodology for particle transport and tracking

In the modeling of microparticle transport, the particle volume fraction relative to the fluid phase was significantly less than 1%, allowing the influence of particles on the fluid to be neglected. Therefore, a one–way coupled Lagrangian discrete-phase model was adopted. In this approach, the airflow field is first simulated at each time step, followed by integrations of the equations of motion for the particles, considering drag and gravitational settling, to track the trajectories of individual particles. The equations representing these models are as follows.

$$\frac{d\vec{u}_p}{dt} = \vec{F}_D + \vec{F}_G + \vec{F}_S \qquad (2)$$

where p denotes the particle phase, and $\vec{F}_D$ represents the drag force per unit particle mass, derived from Stokes' drag law, as expressed in Eq. (3):

$$\vec{F}_D = \frac{(\vec{u}_g - \vec{u}_p)}{\tau} = \frac{18\mu}{\rho_p d_p^2} \cdot \frac{C_D Re_p}{24}(\vec{u}_g - \vec{u}_p) \qquad (3)$$

where μ is the air viscosity, $\vec{u}_g$ is the fluid flow velocity, $\vec{u}_p$ is the particle velocity, d_p is the aerodynamic particle diameter, ρ_p is the particle density, C_D is the drag coefficient, Re_p is the particle Reynolds number.

The second term $\vec{F}_G$ represents the gravitational term. The third term, $\vec{F}_S$, denotes the Saffman lift force, which accounts for the lift owing to shear on a unit mass basis, as expressed in Eq. (4):

$$\vec{F}_S = \frac{2K\nu^{\frac{1}{2}}\rho d_{ij}}{\rho_p d_p (d_{lk} d_{kl})^{\frac{1}{4}}}(\overrightarrow{u_g} - \overrightarrow{u_p}) \qquad (4)$$

where the value of K = 2.594 is a constant, ν is the kinetic viscosity, and d_{ij}, d_{lk}, and d_{kl} are deformation rate tensors.

The turbulent components acting on the particles were modeled using a Discrete Random Walk model, which represents stochastic fluctuations. An idealized wall-trapping condition was applied as the boundary wall, assuming that the particles did not rebound into the flow after colliding with the airway walls. Eleven representative particle sizes were selected to ensure a wide-ranging prediction of particle deposition across microscale sizes, ranging from 1 to 80 μm, and particle density was set to 1,000 kg/m³.

Table-1 Subject scan data of macaques.

Subjects	Body weight (kg)	Age (years)	Gender
Mff765	10.2	28	Female
Mff963	6.6	26	Female
Mff2099	7.0	13	Female
Mff2115	7.9	5	Female
Mff2249	8.0	8	Female

3. Results

3.1. Airflow in the monkey airway models

Fig. 2 shows the steady-state airflow distribution within the airway. Overall, airflow accelerated near the nostrils, decelerated around the central nasal cavity, and rapidly accelerated near the larynx. When comparing individual cases, Mff765, the heaviest of the five subjects, exhibited the highest airflow velocity within the airway.

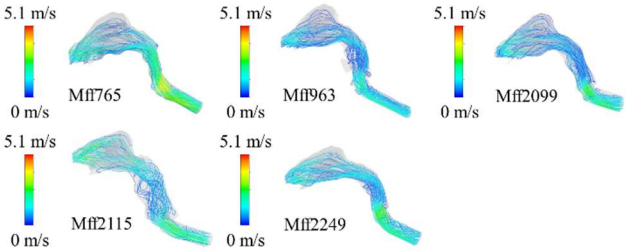

Figure-2 Velocity streamlines distribution in the monkey's upper airways during steady inhalation flow.

3.2. Aspiration efficiency (AE)

Fig. 3 shows various aspiration efficiency (AE) datasets plotted against different particle sizes. AE is defined as the ratio of the concentration of inhaled particles to that of particles in the environment, as shown in Eq. (5):

$$AE = \frac{C_{nostril}}{C_{environment}} = \frac{N_n}{C_{environment} \cdot TV} \qquad (5)$$

where $C_{environment}$ is the particle density in the particle injection box, which corresponds to the particle aspiration zone obtained using the reverse analysis method; TV is the tidal volume; and N_n is the particle inhaled through the nostrils.

Simulation results indicated that Japanese macaques maintained high AE (>0.9) up to 10 μm, with a marked decline from 40 μm owing to gravitational sedimentation. The inter-individual variation was minimal for smaller particles. Among the individuals, Mff963 exhibited the highest efficiency up to 30 μm, whereas Mff765 showed the highest efficiency for larger particles. Across most particle sizes, macaques showed an approximately 0.04 higher efficiency than humans. Nevertheless, the overall trend remained similar, suggesting comparable inhalation behaviors between macaques and humans.

3.3. Particle deposition patterns

Fig. 4 shows particle deposition within the airways of the three representative monkey models with different body weights used in this study. Particle sizes are visualized in different colors: 1, 5, 10, and 30 μm. The 1 μm particles exhibited minimal deposition

across all individuals. In contrast, 5 and 10 μm particles showed significant deposition, predominantly along the floor of the airway, with a particularly pronounced trend in the tracheal region. The nasal cavity had the highest overall particle deposition rate. Additionally, for the 30 μm particles, all were deposited within the nasal vestibule region.

3.4. Particle deposition efficiency (DE)

Fig. 5 presents the five monkeys' deposition efficiency (DE) as a function of the Stokes number. Here, DE (η_a) is defined, as shown in Eq. (6), as the ratio of the number of particles deposited within the airway to the number of particles inhaled through the nostrils.

$$\eta_a = \frac{N_{deposited-airway}}{N_{inhaled-via-nostrils}} \times 100 \qquad (6)$$

where $N_{deposited-airw}$ is the number of particles deposited in the airway, and $N_{inhaled-via-nostril}$ is the number of particles inhaled through the nostrils. The characteristic aspects of the heterogeneous geometrical features of the respiratory tract can be minimized using the Stokes number (Stk), which enables the comparison of various scaling models. The Stokes number was expressed as a function of the aerodynamic diameter d_p, characteristic airflow U, and minimum cross-sectional area A_{min} (Stk $= \rho d_p U/18\mu {A_{min}}^{0.5}$).

To validate the results of this analysis, experimental data obtained from a study by Kelly et al. [3] are included in the figure.

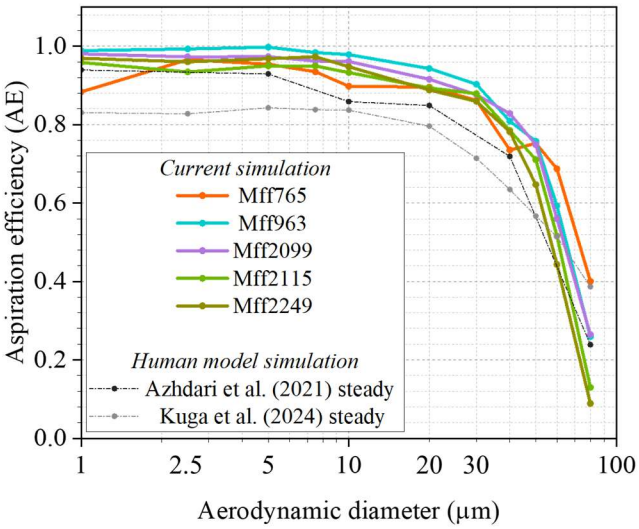

Figure-3 Comparison of aspiration efficiency (AE) as a function of particle size.

The simulation results showed good agreement with the experimental data. The DE in monkeys increased sharply around a Stokes number of approximately 0.01 and reached a peak near 0.1. In terms of inter-individual comparisons, the youngest individual, Mff-2115, exhibited a relatively lower DE up to approximately Stk = 0.1, whereas the oldest individual, Mff-765, showed a notably higher DE around Stk = 0.02 0.05. The DE of macaques was generally slightly higher than that of humans. Overall, particle deposition trends were similar.

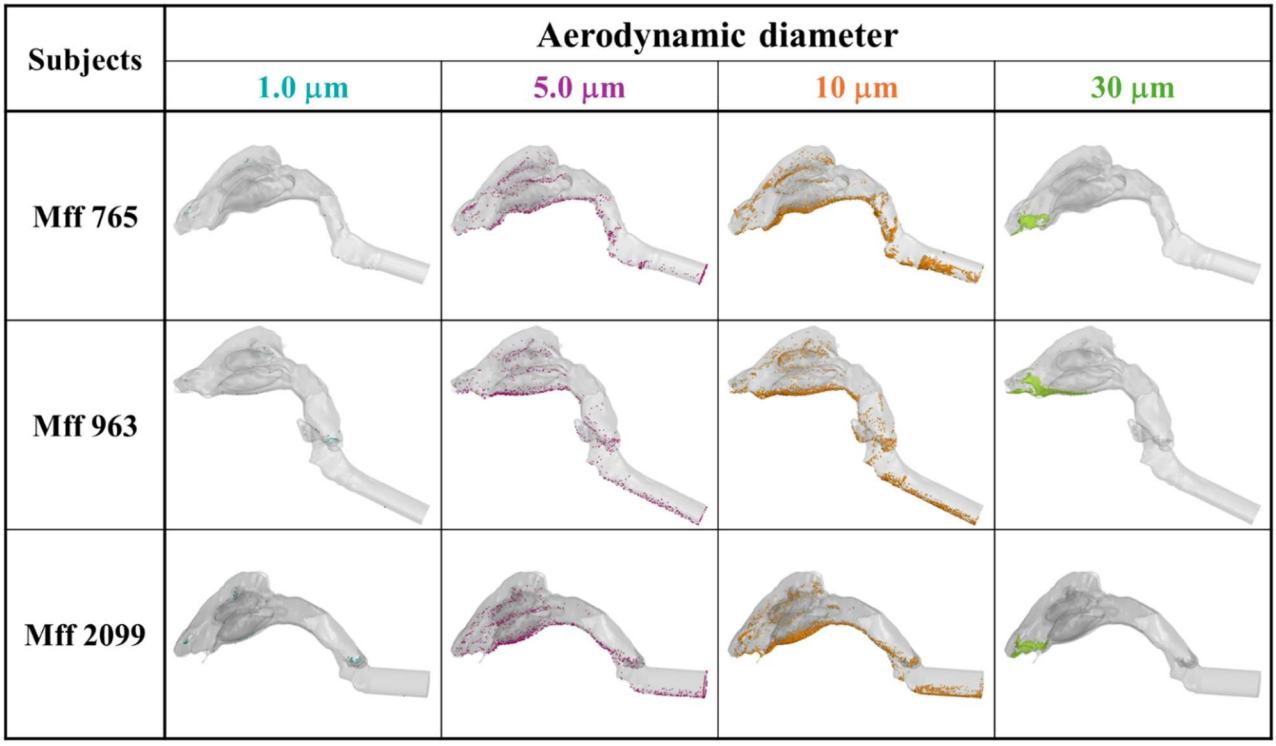

Figure-4 Visualization of micro-particle deposition in the monkey upper airway during steady inhalation (side view).

4. Discussions

In this study, CFPD simulations were conducted using the numerical models of five Japanese macaques with varying individual characteristics. The comparison of AE (Fig. 3) revealed that differences due to body weight were minimal for smaller particle sizes, suggesting that variations in the inhalation velocity had little impact on the aspiration of fine particles. In contrast, substantial differences in the AE were observed for larger particles, where gravitational settling was dominant. Considering the limited number of experimental studies on AE in monkeys, these findings provide valuable insights.

Furthermore, a comparison of DE (Fig. 5) indicated a correlation between age and DE, suggesting that age is a significant factor influencing particle deposition. The Stokes number in this study proved to be a useful tool for comparing particle deposition while accounting for anatomical differences in the airway. The Stokes number is a function that is primarily determined by the characteristic length, characteristic velocity, and particle diameter. The characteristic length and velocity can be approximated as functions of body weight from the perspective of allometric scaling. This indicates the potential of predicting airway deposition based on body weight and particle diameter.

5. Conclusions

In this study, numerical airway models of Japanese macaques (*Macaca fuscata*) were constructed, and CFD simulations were conducted to analyze particle transport and deposition. Comparative analysis with human models was also performed. The key findings are summarized as follows.

I. The airflow within the nasal cavity of Japanese macaques decelerated near the center of the nostrils and subsequently reached a peak velocity in the nasopharyngeal and laryngeal regions.

II. The AE of Japanese macaques remained high (above 0.9) for particle diameters up to approximately 10 μm but decreased sharply for particles around 40 μm, indicating that particles predominantly influenced by gravitational settling are scarcely inhaled.

III. The AE in macaques was slightly higher than that in humans; however, the overall trend in particle aspiration was highly similar between the two species.

IV. Regarding intratracheal particle deposition patterns, 1 μm particles rarely deposited in the airways, whereas 5–10 μm particles deposited throughout the upper airway. Larger particles tend to be deposited entirely in the anterior region of the nasal cavity.

V. The DE in macaques showed a stepwise pattern, increasing around a Stokes number of 0.02 and peaking near 0.1. Differences among individuals were strongly influenced by age-related variations.

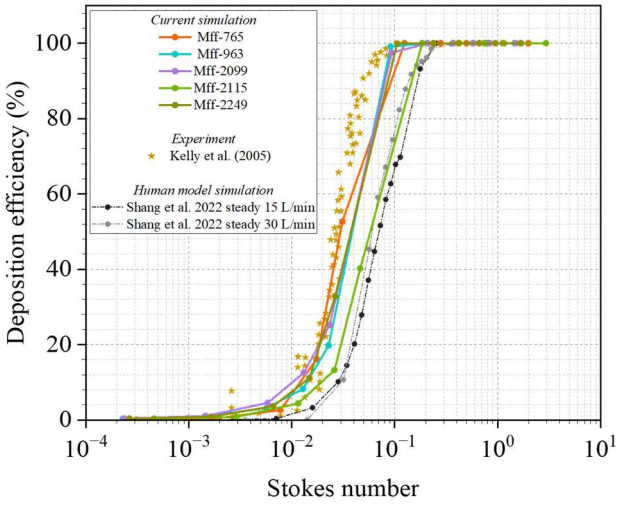

Figure-5 Deposition efficiency in the monkeys compared to experimental results as a function of Stokes number.

Acknowledgments

The authors thank Prof. Nishimura for providing the Computed Tomography (CT) data. This study was also partially funded by the FOREST program of JST, Japan (JPMJFR225R), JSPS KAKENHI (JP 25H00409, JP 22K18300, JP 25K21392, Health, Labour and Welfare Policy Research Grants (JP 24KD2001), and MEXT as a “Program for Promoting Research on the Supercomputer Fugaku” (JPMXP1020210316).

References

1) Karel, L. et al.: Respiration in Macaca mulatta (Rhesus monkey)., *Proceedings of the Society for Experimental Biology and Medicine*, Vol. 61, No.3, pp.291-296, 1946.

2) Azhdari, M. et al.: Particle inhalability of a standing mannequin with large airways in a ventilated room. *Computers in Biology and Medicine*, Vol. 138, 2021.

3) Kuga, K. et al.: Aspiration efficiency and respiratory tract deposition of indoor suspended micro-particles during steady and transient breathings. *Building and Environment*, Vol. 249, 2024.

4) Kelly, J. T. et al.: Inertial particle deposition in a monkey nasal mold compared with that in human nasal replicas. *Inhalation toxicology*, Vol. 17, pp.823-830, 2005.

5) Shang, Y. et al.: Detailed comparative analysis of environmental microparticle deposition characteristics between human and monkey nasal cavities using a surface mapping technique. *Science of the Total Environment*, Vol. 853, 2022.

Energy consumption and CO_2 emissions of motor vehicles: A review

Student Member † Gunadhi ACR (Tokyo City University)
Student Member Hadiwijoyo E (Tokyo City University)
Student Member Arachchi APDT (Tokyo City University)
Member Abdullah N (Tokyo City University)
Member Rijal HB (Tokyo City University)

The transportation sector is one of a major contributor to global carbon dioxide (CO_2) emissions, due to the widespread use of fossil fuel-powered vehicles. This paper presents a comprehensive literature review examining the relation between vehicle energy consumption and CO_2 emissions across various vehicle types and fuel sources. Data were synthesized from 16 case studies, focusing on car, bus, truck, and motorcycle as vehicle type, and gasoline, diesel, electric, and hybrid as fuel type. The analysis reveals that motorcycles exhibit the lowest energy consumption and CO_2 emissions, while buses demonstrate the highest values and greatest variability. Cars and trucks fall within a moderate range for both types of vehicles. Furthermore, the study highlights that electric and hybrid vehicles significantly reduce direct CO_2 emissions compared to conventional gasoline and diesel vehicles. Several factors influencing energy consumption and emissions are discussed, including vehicle condition, driving behavior, road and traffic conditions, and fuel type. The findings underscore the importance of transitioning to cleaner vehicle technologies and improving operational efficiency and productivity to mitigate the environmental impact of transportation.

1. Introduction

Transportation plays a vital role in supporting people's mobility for activities such as studying, working, and daily errands. Common types of transportation include two-wheeled vehicles like bicycles, scooters, and motorcycles, as well as four-wheeled and larger vehicles like cars, buses, and trucks. These vehicles use various energy sources, such as gasoline and diesel (fossil fuels), and increasingly, electricity (batteries). However, the use of gasoline and diesel-powered vehicles has significant negative impacts on the environment [1]. One major issue is air pollution, caused by emissions released from engines and exhaust systems, and these emissions often contain harmful substances like Carbon Monoxide (CO), Carbon Dioxide (CO_2), Nitrogen Oxides (NOx), Hydrocarbons (HC), and Sulfur Dioxide (SO_2), which can be dangerous to human respiratory health and the environment [2]. The one which affects the environment because its effect relates to Green House Gas is Carbon Dioxide (CO_2). In 2022, global CO_2 emissions from energy combustion and industrial processes grew by 0.9% and reached a record high of emissions 36.8 billion metric tons [3]. To avoid the global CO_2, controlling vehicle dependence on fossil fuels is the most appropriate alternative to significantly reduce CO_2 emissions from the transportation sector [4]. This is because electric vehicles when operated do not produce direct exhaust emissions such as CO_2, NOx, and other particles that contribute to air pollution [5]. This is because electric vehicles use electric motors powered by lithium-ion batteries, without the combustion process of fossil fuels so that the results of CO_2 emissions are generated from power generation sources such as Steam Power Plant which is used as a source of energy to charge batteries in electric vehicles [6].

The reported CO2 emissions and Energy consumption values for vehicles vary across different studies in different contexts, found as a critical gap in understanding the overall impact of vehicle type and fuel type on energy consumption and CO_2 emissions. By conducting meta-analysis this study will examine the average values of CO_2 emissions and energy consumption based on vehicle type and fuel type, as well as the largest contributor to CO_2 emissions in whole world scenario.

2. Methodology

2.1. Data collection

In this research, a literature review method was used relating to the correlation between the level of energy consumption used and the total amount of emissions released by both motorized and electric vehicles. The literature review used the keywords "energy consumption" and "emissions of gasoline/diesel and electric vehicles" referring to 490 journals found on Scopus and Google Scholar, and obtained 16 relevant journals [7-22]. The literatures included must have these requirements: data on the type of vehicle, the type of propulsion energy (whether gasoline / diesel or electricity), the number of vehicles, the fuel or electric consumption, the vehicle mileage, the emission factor, the amount of CO_2 emissions, and the amount of energy consumption.

2.2. Calculations

The value of energy consumption and CO_2 emissions following equations were used.

$$E = \frac{Fc}{D} \quad (1)$$

$$Q = \frac{W}{D} \qquad (2)$$

Where:

E : Energy consumption (liter/km) W: Weight of CO_2 (g)

D : Vehicle mileage (km) Q: CO_2 emissions (g/km)

Fc : Fuel consumption (liter)

3. Results and discussion

3.1. Energy consumption

Energy consumption in a gasoline or diesel vehicle refers to the amount of fuel (gasoline or diesel) used to travel a specific distance, commonly expressed as liters per 100 kilometers (liter/100km) or per kilometers (liter/km) [23]. While energy consumption in an electric vehicle (EV) is defined as the amount of electrical energy used to travel a specific distance, typically measured in kilowatt-hours per 100 kilometers (kWh/100 km) or per km (kWh/km) [24].

In Figure 1 the distribution of energy consumption is explained that the higher energy consumption amount, the lower the number of samples. This means that most vehicles sampled in previous studies have small energy consumption values and certainly will reduce the use of excess fuel.

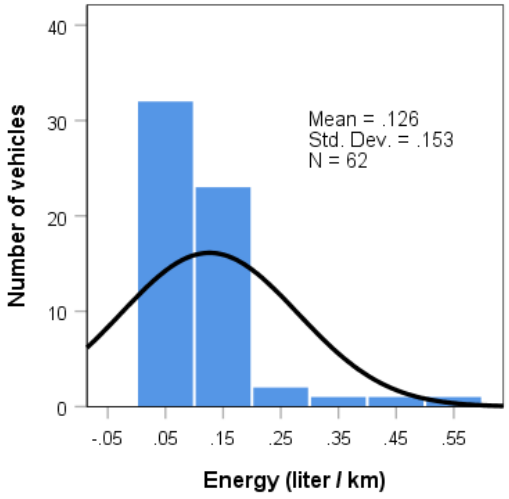

Figure 1. Distribution of energy consumption

Furthermore, Figure 2 explains of different type energy consumption whereby buses the energy consumption range of buses is between 0.1 to almost 1 liter/km, which is quite large and high, and motorcycles have the energy consumption range of between 0.02 to 0.1 liter/km reflecting a vehicle that has the lowest energy consumption and is more energy efficient.

Several factors are analysed that cause high energy consumption including vehicle and condition, driving method, road condition, and vehicle load. For example, if the vehicle conditions are not in good condition such as when the vehicle is used when the tires are flat, improper driving methods such as using the acceleration often than usual, road conditions such as uphill or downhill prompting drivers to do more braking and acceleration repetitively, and excessive vehicle loads such as carrying a lot of cargo will force the vehicle to use energy from fuel or electricity to keep moving [25].

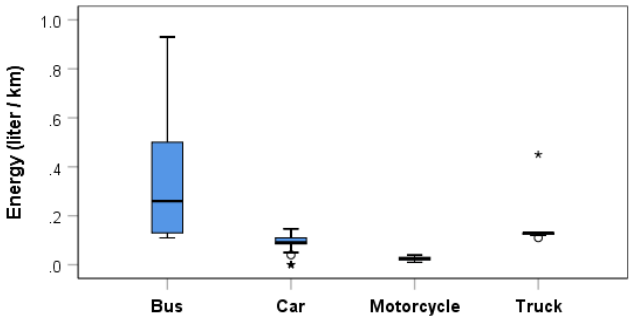

Figure 2. Energy consumption per vehicle type

3.2 CO_2 emission

The main source of CO_2 from gasoline and diesel vehicles is the fuel in the engine. CO_2 emission of vehicles is measured in grams of CO_2 emitted per individual per kilometer, or we can mention as g/km [26]. Meanwhile, CO_2 emissions in electric vehicles are defined as the result of the use of electrical energy divided by mileage [13].

Figure 3 explains the distribution of vehicle that higher the CO_2 amount, the lower number of samples. This means that most vehicles sampled in previous studies have small to medium CO_2 emissions values.

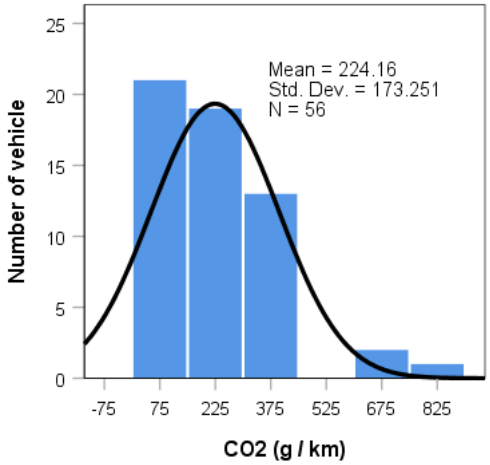

Figure 3. Distribution of CO_2 emission

Figure 4 shows the amount of CO_2 emissions by vehicle type. Buses produce exceptionally large amount of CO_2 emissions, which is around 350 to 400 g/km, and motorcycles produces the smallest amount of CO_2 emissions, which is around 100 g/km.

Several factors are analysed that cause high CO_2 emissions including vehicle type, fuel, and its age. Variations in small and

large vehicle types both from the vehicle body and engine capacity, the type of fuel and its octane number whether it is in accordance with the type of vehicle, and how old the vehicle and its maintenance will affect CO_2 gas levels in the exhaust gas [27].

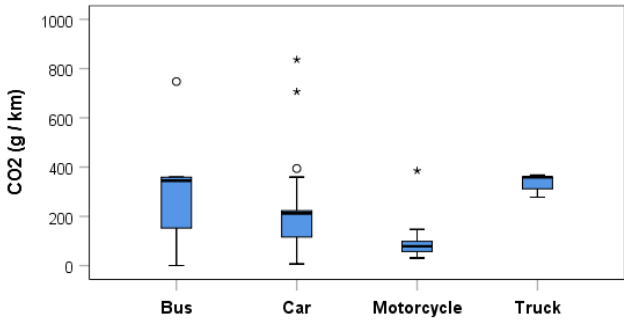

Figure 4. CO_2 emission per vehicle type

3.3 Relation between CO_2 emission and energy consumption

Current energy consumption trends which are increasing much faster indicate that the environmental and social costs caused by CO_2 in 2025 follow an upward trend and will contribute to CO_2 emissions. [28].

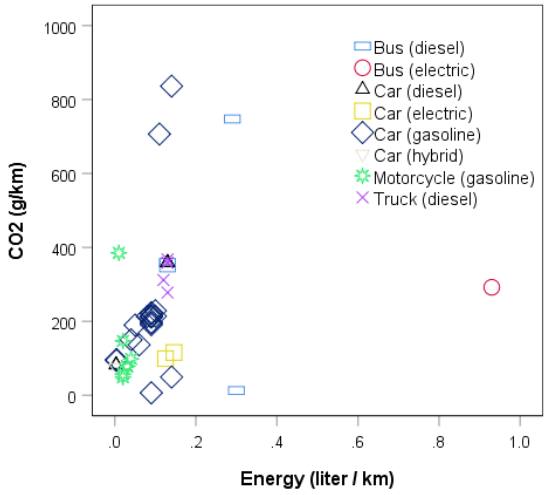

Figure 5. Relation between energy consumption and CO_2 emission for each vehicle

Figure 5 shows the relationship between the amount of CO_2 emissions and energy consumption produced by each type of vehicle. Motorcycles have the smallest energy consumption with an energy consumption of 0.1 liter/km, and buses (electric) have the highest energy consumption compared to all other vehicles, with energy consumption of almost 1 liter/km. In other side, cars (gasoline) have the smallest CO_2 emissions of 50 g/km and highest CO_2 emissions compared to all other vehicles, with CO_2 emissions of 900 g/km.

Based on the results above, the type of vehicle also affects the amount of energy consumption and CO_2 emissions it emits. Motorcycles have a small chassis body size and engine capacity and can only be occupied by a maximum of 2 people so that they do not require large fuel consumption to operate and it can reduce the CO_2 emission on their tailpipes. In contrast, buses (electric) have a large chassis body and engine capacity and are used to transport many people so that operating at larger loads requires large energy consumption and the CO_2 production will increase.

3.4. Contribution to global CO_2 emissions

To identify the major contributors to global CO_2 emissions, we estimated the number of vehicles currently in use in the world using different sources.

Table 1. Estimated annual contribution of CO_2 for each vehicle type globally: 2025

Vehicle Type	Estimated global number (millions)	Average annual distance (km)	Mean CO_2 (g/km)	Total CO_2 emissions (g/km) millions
Motorcycle: gasoline	662 [29]	10,058 [37]	108.20	720,438,447.20
Car: diesel	591.9 [30]	21,726 [38]	266.86	3,431,718,033.08
Car gasoline	900 [31]	21,726 [38]	231.60	4,528,567,44
Car: hybrid	60 [32]	21,093 [39]	75.00	94,918,500
Car: electric	50 [33]	16,334 [39]	107.49	87,787,083
Truck: diesel	200 [34]	22,128 [38]	335.00	1,482,576,000
Bus: diesel	16 [35]	56,327 [38]	303.85	273,839,343.20
Bus: electric	0.7 [36]	56,327 [38]	292.10	11,517,181.69

Table 1 shows the estimated CO_2 emissions for each vehicle type using the estimated number of vehicles and distance per year. From these results we can conclude that the largest CO_2 contributor is cars (gasoline) with a total of 4,5285,567.44 million g/km per year and the smallest is electric buses with a total of 11,517,181.69 million g/year, respectively. This indicates even considerable number of electric and hybrid vehicles in the use, still large portion of transportation sector depend on fossil fuels. Oluwole et al. [40] said that the overpopulation of passenger vehicles (cars) has a negative impact on the environment, therefore, to reduce the impact of fossil fuel-based vehicles, it is necessary to promote switching to other environmentally friendly public vehicles.

4. Conclusions

1. Based on the extensive literature reviews, motorcycles and electric bus are found to have low energy consumption and low CO_2 emission as compared to other vehicles.
2. The condition of vehicles with top engine performance, adopt driving methods that are in accordance with operating procedures, good road and contour conditions, and a small vehicle load may reduce the high energy consumption of the vehicle.
3. By using vehicles that are sized according to needs, fuel that is suitable for the vehicle engine designation, and vehicle maintenance methods that are on time and in a way that will support the reduction of CO_2 emissions in vehicles.
4. The largest CO_2 contributor is cars (gasoline) and the smallest is electric buses.

Acknowledgement

The authors would like to thank to the MEXT Scholarship for providing the opportunity to conduct this research.

References

[1] Fayyazbakhsh et al. (2022). *Journal of Cleaner Production*. 376,1-19.

[2] Resitoglu et al. (2014). Journal of *Clean Technologies and Environmental Policy*. 17,15-27

[3] United Nation. (2023). Sustainable Development Goals Report 2023: Special Edition. *United Nation*. 1(1).

[4] Wang et al. (2022). *Research Square*.

[5] US Department Energy. (2025). Emissions from Electric Vehicle. https://afdc.energy.gov/

[6] Ferlita et al. (2023). *Journal of Physics Education*. 7(2), 356-365.

[7] Fitrianto H. (2023). *Repository IMWI*. 6(2),1056-1067.

[8] Dinar et al. (2022). *Journal of Applied Geomining and Metallurgy*. 2(1),42-61.

[9] Sari et al. (2021). *Journal of Geoscience*. 6(4),234-242.

[10] Ambarsari et al. (2019). *Journal of Planning for Urban Region and Environment*. 8(1),183-194.

[11] Rachman et al. *Journal of Mechanical Engineering: Dynamic*. 8(1),49-58.

[12] Serlina et al. (2024). *Journal of Serambi Engineering*. 9(3),9889-9897.

[13] Brockdorff et al. (2017). *Journal of Case Studies on Transport Policy*. 5,509-517).

[14] Peng et al. (2015). *Journal of Energy Conversion and Management*. 102,4-16.

[15] Ong et al. (2011). *Journal of Renewable and Sustainable Energy Reviews*. 15,3516-3522.

[16] Bose et al. (1997*). Journal of Energy Policy*. 25,14-15).

[17] Baeza et al. (2014). *Journal of Energy*. 66,624-634.

[18] Li et al. (2022). *Journal of MDPI: Sustainability*. 14,1-16.

[19] Ko et al. (2014). *Journal of Transportation Research*. 59,346-356.

[20] Saptoadi H. (2016). *AIP Conference Proceedings*. doi: 10.1063/1.4958535.

[21] Machado et al. (2020). *Energies*. 13,5433.

[22] Grijalva et al. (2019). *Energies*. 12,525.

[23] ACE Mechanics. (2025). Understanding Fuel Consumption and Fuel Efficiency: http://www.acemechanics.com.au/blog/understanding-fuel-consumption-and-fuel-efficiency/

[24] Electric Vehicle (EV) Life. (2025). Available from: http://evlife.world/tech/how-does-ev-power-consumption-information-work/

[25] Wiratama Mitra Abadi. (2025). http://wma.co.id/articles/pentingnya-sistem-fuel-consumption-untuk-meningkatkan-efisiensi-bahan-bakar/

[26] Visual Capitalism. (2022). http://www.visualcapitalist.com/comparing-the-carbon-footprint-of-transportation-options/

[27] Rusdiani et al. (2018). *Repository ITS*. 1,1-75.

[28] Mirzaei et al. (2017). *Journal of Environmental Research.* 154,345-351.

[29] Marklines. (2023). https://www.marklines.com/en/report/rep2529_202308

[30] Global Diesel Vehicle Market: Forecast 2025-2031. (2025).: https://www.gii.co.jp/report/qyr1724624-global-diesel-cars-market-size-manufacturers.html

[31] https://hedgescompany.com/blog/2021/06/how-many-cars-are-there-in-the-world/

[32] Anjali L. (2024).https://www.cognitivemarketresearch.com/hybrid-vehicles-market-report

[33] IEA. (2025). https://www.iea.org/reports/global-ev-outlook-2025/trends-in-electric-car-markets-2

[34] 2025 Global Outlook for Heavy-Duty Trucks Isn't Rosy. (2024). https://www.spglobal.com/ratings/en/research/articles/241211-2025-global-outlook-for-heavy-duty-trucks-isn-t-rosy-13354457

[35] IEA. Trucks and Buses. https://www.iea.org/energy-system/transport/trucks-and-buses

[36] Takahashi M. (2024). https://www.idtechex.com/en/research-report/electric-and-fuel-cell-buses-2025-2045-markets-players-technologies-and-forecasts/1012

[37] Dinesh et al. (2014). *Energy, Climate, and Sustainability Development.* 1,1-38.

[38] US Department Energy. (2025) https://afdc.energy.gov/data

[39] MIT Climate Portal. (2023). https://climate.mit.edu/posts/how-much-are-electric-vehicles-driven-depends-ev

[40] Oluwole et al. (2022). *Journal of Energy Report.* 8,2052-2061.

Hybrid IPSO–Adam Optimization for Data-Driven Model-Based Air-Balancing Control

Student Member †Shanrui SHI (The University of Tokyo) Member Shohei MIYATA (The University of Tokyo)
SHASE Technical Fellow Yasunori AKASHI (The University of Tokyo)

This study proposes a data-driven, model-based control strategy for optimal air balancing in multizone ventilation systems. An artificial neural network (ANN) surrogate is trained on simulation data to model duct airflow, and a hybrid IPSO–Adam optimizer is used to compute energy-efficient control inputs under operational constraints. Compared with traditional trim-and-respond control and other benchmark strategies, the proposed method achieves faster setpoint recovery, higher airflow accuracy, and lower fan energy use. It also requires only airflow measurements, reducing sensor and tuning requirements. The approach is well-suited for future transfer learning and real-world application.

Introduction

Demand-controlled ventilation (DCV) dynamically modulates airflow based on real-time indoor conditions to maintain indoor air quality (IAQ) and energy efficiency. In systems equipped with CO_2 sensors, the control strategy maintains indoor concentrations below a prescribed threshold. In contrast, systems without gas sensors typically rely on measured or forecasted occupancy patterns to schedule airflow [1]. This latter approach—commonly referred to as *air balancing*—aims to align the delivered outdoor airflow with a zone's instantaneous demand, minimizing control error [1]. Achieving precise air balancing in multi-zone buildings remains challenging due to complex duct interactions, which often cause substantial discrepancies between the intended and actual airflow rates at terminal units [1]. These discrepancies can lead to underventilation, compromising IAQ, or overventilation, resulting in unnecessary fan energy consumption. Therefore, the development of air-balancing control strategies that are both energy-efficient and accurate is of practical importance.

Data-driven approaches, which learn system dynamics directly from operational data, have demonstrated superior performance over conventional rule-based and physics-based methods. As a state-of-the-art example, Cheng et al. [2] proposed an end-to-end neural network that embeds energy-saving constraints, while Li et al. [3] extended this work by incorporating multiple constraints into an improved perceptron formulation. However, these methods rely heavily on kernel-based models, which may have limited capacity in representing complex, high-dimensional, or highly nonlinear duct systems. Furthermore, their penalty-based constraint implementation enlarges the optimization landscape and increases sensitivity to hyperparameters, leading to higher computational costs.

To overcome these challenges, this study proposes a data-driven, model-based optimal air-balancing control strategy that ensures accurate airflow distribution and energy-efficient operation in complex duct networks. Data-driven models often require large volumes of high-quality operational data, which can be costly and time-intensive to collect. A practical solution is to adopt a sim-to-real training scheme, in which data generated from a physical system model is used for initial training, followed by fine-tuning with a small amount of real-world data. While the present study uses only simulation data, it establishes the foundation for future transfer learning. Therefore, a key objective is to develop a data-driven model that captures the essential dynamics of the ventilation system and exhibits generalization capability for real-world adaptation and deployment.

1. Proposed data-driven model-based optimal air-balancing control strategy

1.1 Modelica-based system model

As shown in Fig. 1, the target system is a hypothetical setup based on the experimental configuration described in [4]. A detailed physics-based model (Fig. 2) of the system was developed using the Modelica Buildings Library [5] and simulated on the OpenModelica platform. The model was then exported as a Functional Mock-up Unit (FMU) and co-simulated from Python using the FMPy package.

1.2 ANN surrogate model

An artificial neural network (ANN) model was trained to learn the nonlinear mapping between actuator inputs and the resulting airflow distribution across the duct network. A five-layer multilayer perceptron (MLP) with three hidden layers was adopted, as shown in Fig. 3. Using the FMU, a total of $4^7 = 16384$ input-output samples were generated through random sampling. The ANN was trained following the procedures described in [6].

1.3 Optimal air-balancing control formulation

Once the surrogate model is trained, the optimal control problem at each time step is formulated as:

$$\min J = \sum_{i=1}^{6}(Q_i - Q_i^{\text{set}})^2 + \lambda + w * inv_{\text{SA}} \quad (1)$$

The first term penalizes deviations between the predicted airflow Q_i and the setpoint Q_i^{set}, which is derived from real-time occupancy. The second term λ is a constraint penalty ensuring that at least one damper remains nearly fully open (i.e., >0.85) to minimize system resistance. The third term penalizes fan power usage, scaled by the weighting factor w.

Given the non-convex and highly nonlinear nature of the problem, a hybrid IPSO-Adam algorithm is used to solve it. An improved particle swarm optimization (IPSO) method with a double linearly decreasing inertia weight [7] performs a global search to find a feasible initial solution. This is followed by local refinement using the Adam optimizer [8], which exploits the analytical gradients of the surrogate model for efficient convergence. Since the damper constraint term λ in Eq. 1 is non-differentiable, it poses challenges for gradient-based solvers. While IPSO handles this without issue, the Adam stage may become trapped in non-smooth regions. To address this, the constraint is relaxed using a ReLU-based penalty function:

$$\lambda = \lambda' \text{ReLU}(0.85 - \max d_i) \quad (2)$$

Here, λ' is a penalty coefficient enforcing the constraint. Furthermore, early stopping is applied during Adam optimization to terminate the process when the objective fails to improve by a predefined threshold over a set number of iterations. The whole optimization framework is shown in Fig. 4. This hybrid approach combines the global search capability of PSO with the fast, gradient-based refinement of Adam, achieving accurate and energy-efficient air balancing with runtimes compatible with real-time implementation.

2. Validation test arrangement

2.1 Test conditions

Simulation experiments were conducted to evaluate the proposed optimal air-balancing strategy. The only external input was the six-zone occupancy schedule (Fig. 5). Based on the instantaneous number of occupants P_i in each zone, the outdoor-air ventilation setpoint Q_i^{set} is computed using the ASHRAE Standard 62.1 method [9]: $Q_i^{\text{set}} = R_z A_i + R_P P_i$, where $A_i = 76.8\text{m}^2$ is the zone floor area, $R_z = 0.30\text{L}/(\text{s}\cdot\text{m}^2)$ is the area-based ventilation rate, and $R_P = 2.5\text{L}/(\text{s}\cdot\text{person})$ is the per-person ventilation rate.

2.2 Control strategies for comparison

Strategy 1*: *Trim-and-Respond (TR). Based on ASHRAE Guideline 36 [10], each zone damper is regulated by a PI loop to track Q_i^{set} Fan static pressure is adjusted via *Trim* (decrease when all dampers are lower than 85%) and *Respond* (increase

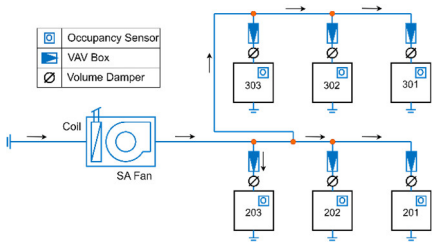

Figure-1: Schematic of the six-room ventilation system.

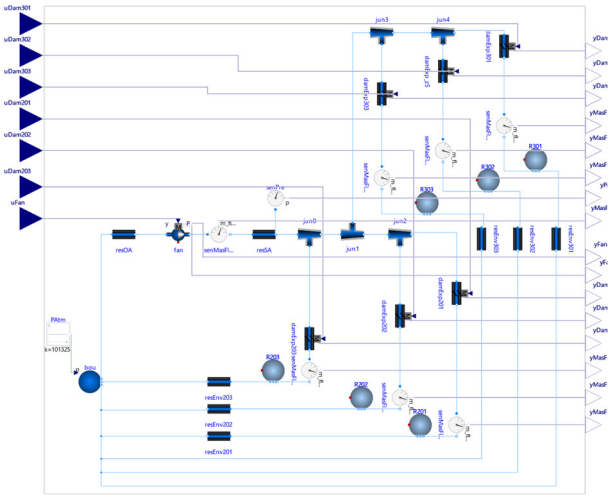

Figure-2: Modelica model of the ventilation system.

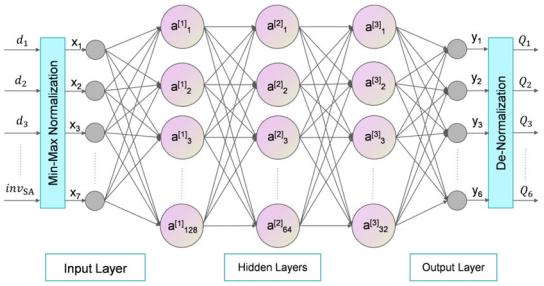

Figure-3: Structure of the developed ANN surrogate model.

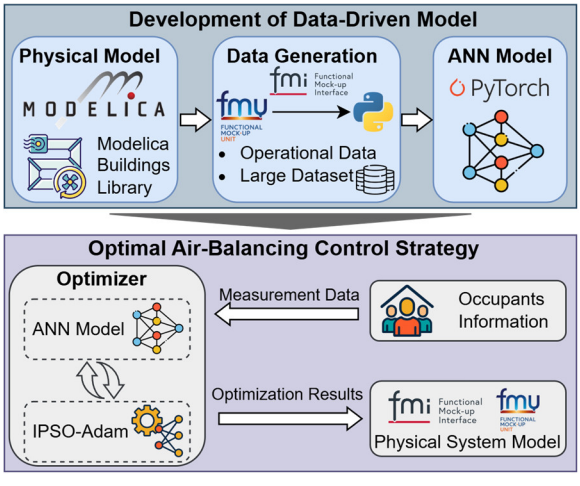

Figure-4: Framework of the proposed strategy.

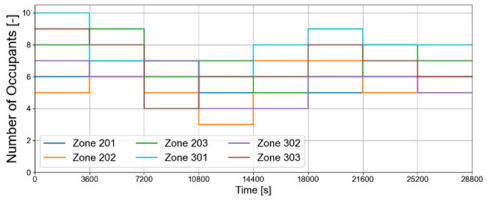

Figure-5: Occupancy schedule used in the test case.

when any damper exceeds 95%). Controllers were manually tuned and implemented in Python with the same FMU. ***Strategy 2*: *Sole IPSO***. Uses only the IPSO algorithm for optimization. The number of particles and iterations were increased for performance. Other parameters matched the proposed method. ***Strategy 3*: *Sole Adam***. Uses only the Adam optimizer. To mitigate sensitivity to initialization, optimization was repeated 10 times per step, selecting the best result. Each step used the previous step's output as initialization. ***Strategy 4*: *Unconstrainted IPSO-Adam***. This strategy is identical to the proposed hybrid approach but omits the damper and fan frequency constraints. All optimization parameters and settings remained the same as in the proposed method. ***Strategy 5*: *Proposed IPSO-Adam***. This is the full hybrid strategy combining IPSO with Adam, as described in Section 1.3. All hyperparameters were tuned through a trial-and-error process to balance convergence speed and control accuracy.

3. Test results and performance comparison

3.1 Fan frequency and damper behavior

As shown in Fig. 6, Strategy 1 adjusts the fan pressure setpoint through trim-and-respond logic to keep the most open damper within recommended range. However, prolonged periods with all dampers below 85% lead to higher system pressure losses and increased fan energy consumption. Strategy 2, given sufficient particles and iterations, successfully maintains at least one damper fully open. Strategy 3 is highly sensitive to initial values--effective when initialized well, but prone to failure otherwise. Strategy 4 often meets the damper constraint indirectly, as IPSO occasionally identifies feasible positions that Adam then refines. However, without explicit constraints, performance is not guaranteed. In contrast, Strategy 5 explicitly enforces constraints and consistently maintains optimal damper openings, resulting in more robust control. Furthermore, the reactive nature of TR leads to noticeable damper hunting even when zone setpoints are stable, and it is exacerbated by actuator lag between control signals and realized damper positions. Model-based strategies (Strategies 2-5) offer smoother operation and faster response.

3.2 Zone airflow control accuracy

Figure 7 presents the absolute percentage error (APE) between achieved and target airflow rates for each zone. Strategy 1 generally keeps APE under 10% but exhibits slow stabilization after occupancy changes. Strategy 2 may converge to local minima, yielding suboptimal results. Strategy 3 performs well with multiple restarts and warm starts but degrades under largely changing conditions. Strategies 4 and 5 consistently deliver the most accurate balancing, demonstrating the benefit of combining global and local optimization with constraint handling.

3.3 Summary of performance

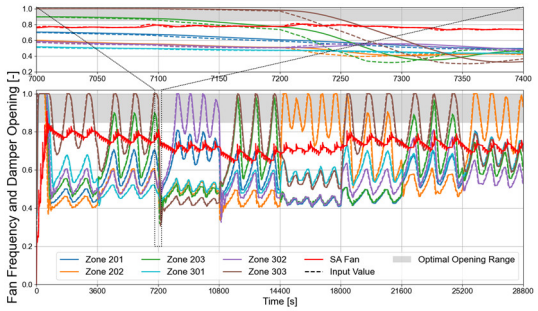

(a) Strategy 1: TR.

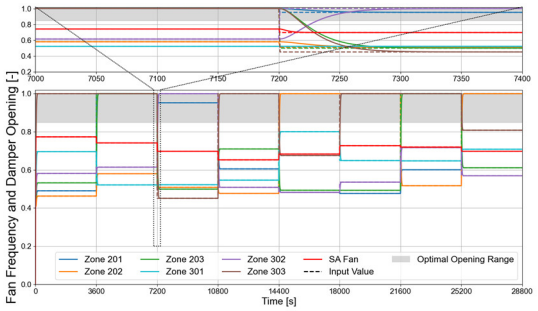

(b) Strategy 2: Sole IPSO.

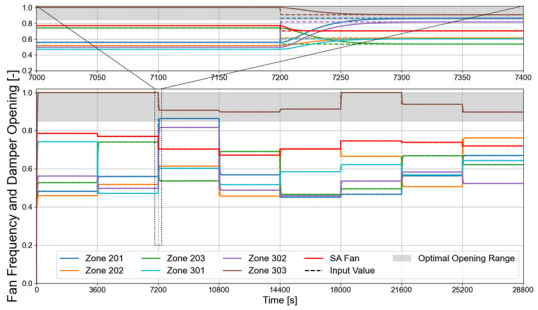

(c) Strategy 3: Sole Adam.

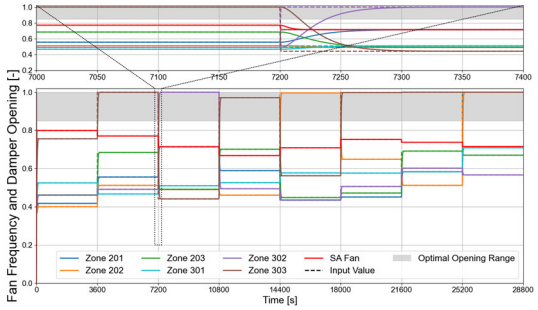

(d) Strategy 4: Unconstrainted IPSO-Adam.

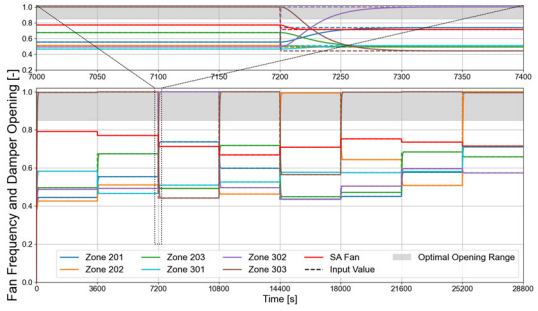

(e) Strategy 5: Proposed IPSO-Adam.

Figure-6: Operational behavior of damper openings and fan frequencies using different control strategies. (Top: zoomed-in view.)

Table 1 summarizes overall performance. Control accuracy is measured by the mean absolute percentage error (MAPE) across all zones. Additional metrics include total supply air (SA) deviation from the 8104 m^3 reference, fan energy consumption, and average computation time per control step. Strategy 1 showed the highest MAPE, while Strategies 2 and 3 improved accuracy but exhibited occasional under- or over-ventilation. Strategy 5 consistently outperformed all others, achieving the best control accuracy, energy efficiency, and runtime feasibility.

4. Conclusion

This study presented a data-driven, model-based air-balancing control strategy that combines an ANN surrogate model with a hybrid IPSO-Adam optimizer incorporating energy-saving constraints. Simulation results demonstrate three key advantages: (1) The strategy recovers to new setpoints within two minutes and maintains high airflow balancing precision. (2) By keeping at least one damper fully open and reducing fan frequency, it minimizes pressure losses and fan energy use. (3) Unlike TR control, it requires only airflow measurements, avoiding pressure sensors and PI tuning. The proposed approach offers an efficient solution for real-time air balancing, with potential for real-world deployment through transfer learning.

Acknowledgements

This work was supported by JSPS KAKENHI Grant Number JP25KJ1173.

This study was conducted as part of the "Smart Building System Research Initiative." The authors would like to thank all individuals involved in this study.

References

[1] Li, Bingxu. "Advanced demand-controlled ventilation strategies for ACMV systems." (2022).

[2] Cheng, Fanyong, et al. "A novel data-driven air balancing method with energy-saving constraint strategy to minimize the energy consumption of ventilation system." *Energy* 239 (2022): 122146.

[3] Li, Lingzhi, et al. "A novel air balancing method based on an improved perceptron under multiple constraints for the energy conservation of ventilation system." *Building and Environment* 248 (2024): 111115.

[4] Shi, Shanrui, et al. "Model-based optimal control strategy for multizone VAV air-conditioning systems for neutralizing room pressure and minimizing fan energy consumption." *Building and Environment* (2024): 111464.

[5] Wetter, Michael, et al. "Modelica buildings library." *Journal of Building Performance Simulation* 7.4 (2014): 253-270.

[6] Shi, Shanrui, Shohei Miyata, and Yasunori Akashi. "Event-driven model-based optimal demand-controlled ventilation for multizone VAV systems: Enhancing energy efficiency and indoor environmental quality." *Applied Energy* 377 (2025): 124683.

[7] Farooq, Mehr Umer, Akhlaque Ahmad, and Abdul Hameed. "Opposition-based initialization and a modified pattern for Inertia Weight (IW) in PSO." *2017 IEEE International Conference on INnovations in Intelligent SysTems and Applications (INISTA)*. IEEE, 2017.

[8] Kingma, Diederik P., and Jimmy Ba. "Adam: A method for stochastic optimization." *arXiv preprint arXiv:1412.6980* (2014).

[9] ASHRAE. "ANSI/ASHRAE Standard 62.1-2010: Ventilation for Acceptable Indoor Air Quality. " *American Society of Heating, Refrigerating, and Air-Conditioning Engineers, Atlanta* (2010).

[10] ASHRAE, Guideline. "36: High performance sequences of operation for HVAC systems." *American Society of Heating, Refrigerating and Air - Conditioning Engineers, Atlanta* (2024).

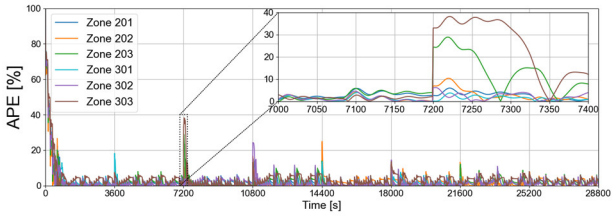

(a) Strategy 1: TR.

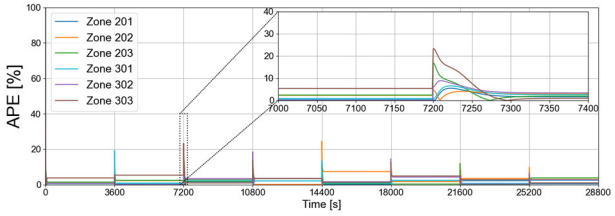

(b) Strategy 2: Sole IPSO.

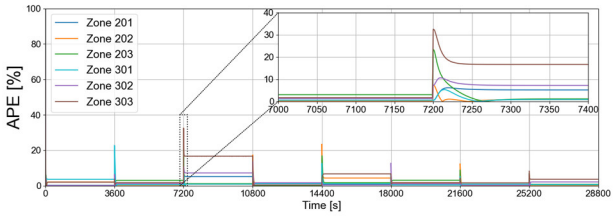

(c) Strategy 3: Sole Adam.

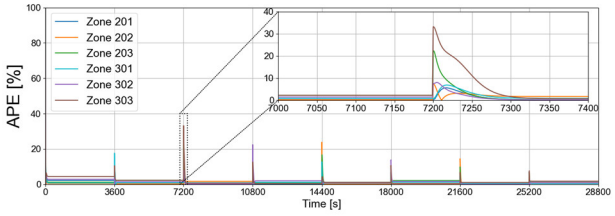

(d) Strategy 4: Unconstrainted IPSO-Adam.

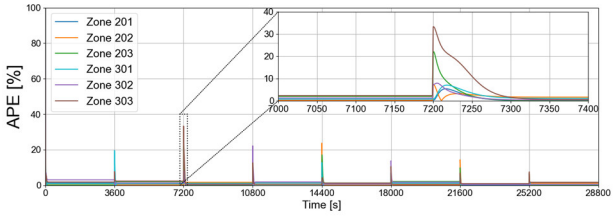

(e) Strategy 5: Proposed IPSO-Adam.

Figure-7: Absolute percentage error (APE) of zone airflows.

Table 1: Summary of control performance for each strategy.

Strategy	MAPE [%]	Total SA Deviation [%]	Energy [kWh]	Running Time [s]
TR	2.48	-0.71	0.976	Real-time
Sole IPSO	2.13	-1.98	0.907	4.16
Sole Adam	1.91	0.24	0.980	0.29
Unconstrained IPSO-Adam	1.09	-0.02	0.993	0.65
Proposed IPSO-Adam	**1.00**	**-0.02**	**0.988**	**0.76**